SKI Report 2005:27

Research

DECOVALEX III/BENCHPAR PROJECTS

Approaches to Upscaling Thermal-Hydro-Mechanical Processes in a Fractured Rock Mass and its Significance for Large-Scale Repository Performance Assessment

Summary of Findings

Report of BMT2/WP3

Compiled by:
Johan Andersson
Isabelle Staub
Les Knight

February 2005

ISSN 1104–1374
ISRN SKI-R-05/27-SE

SKI

SKI Report 2005:27

Research

DECOVALEX III/BENCHPAR PROJECTS

Approaches to Upscaling Thermal-Hydro-Mechanical Processes in a Fractured Rock Mass and its Significance for Large-Scale Repository Performance Assessment

Summary of Findings

Report of BMT2/WP3

Compiled by:
Johan Andersson[1]
Isabelle Staub[2]
Les Knight[3]

[1]JA Streamflow AB, Älvsjö, Sweden
[2]Golder Associates AB, Stockholm, Sweden
[3]Nirex UK Ltd, Oxon, United Kingdom

February 2005

This report concerns a study which has been conducted for the DECOVALEX III/ BENCHPAR Projects. The conclusions and viewpoints presented in the report are those of the author/authors and do not necessarily coincide with those of the SKI.

Foreword

DECOVALEX is an international consortium of governmental agencies associated with the disposal of high-level nuclear waste in a number of countries. The consortium's mission is the DEvelopment of COupled models and their VALidation against EXperiments. Hence theacronym/name DECOVALEX. Currently, agencies from Canada, Finland, France, Germany, Japan, Spain, Switzerland, Sweden, United Kingdom, and the United States are in DECOVALEX. Emplacement of nuclear waste in a repository in geologic media causes a number of physical processes to be intensified in the surrounding rock mass due to the decay heat from the waste. The four main processes of concern are thermal, hydrological, mechanical and chemical. Interactions or coupling between these heat-driven processes must be taken into account in modeling the performance of the repository for such modeling to be meaningful and reliable.

The first DECOVALEX project, begun in 1992 and completed in 1996 was aimed at modeling benchmark problems and validation by laboratory experiments. DECOVALEX II, started in 1996, built on the experience gained in DECOVALEX I by modeling larger tests conducted in the field. DECOVALEX III, started in 1999 following the completion of DECOVALEX II, is organized around four tasks. The FEBEX (Full-scale Engineered Barriers EXperiment) in situ experiment being conducted at the Grimsel site in Switzerland is to be simulated and analyzed in Task 1. Task 2, centered around the Drift Scale Test (DST) at Yucca Mountain in Nevada, USA, has several sub-tasks (Task 2A, Task 2B, Task 2C and Task 2D) to investigate a number of the coupled processes in the DST. Task 3 studies three benchmark problems: a) the effects of thermal-hydrologic-mechanical (THM) coupling on the performance of the near-field of a nuclear waste repository (BMT1); b) the effect of upscaling THM processes on the results of performance assessment (BMT2); and c) the effect of glaciation on rock mass behavior (BMT3). Task 4 is on the direct application of THM coupled process modeling in the performance assessment of nuclear waste repositories in geologic media.

On September 25, 2000 the European Commission (EC) signed a contract of FIKW-CT2000-00066 "BENCHPAR" project with a group of European members of the DECOVALEX III project. The BENCHPAR project stands for ´Benchmark Tests and Guidance on Coupled Processes for Performance Assessment of Nuclear Waste Repositories´ and is aimed at improving the understanding to the impact of the thermo-hydro-mechanical (THM) coupled processes on the radioactive waste repository performance and safety assessment. The project has eight principal contractors, all members of the DECOVALEX III project, and four assistant contractors from universities and research organisations.The project is designed to advance the state-of-the-art via five Work Packages (WP). In WP 1 is establishing a technical auditing methodology for overseeing the modeling work. WP´s 2-4 are identical with the three bench-mark tests (BMT1 - BMT3) in DECOVALEX III project. A guidance document outlining how to include the THM processes in performance assessment (PA) studies will be developed in WP 5 that explains the issues and the technical methodology, presents the three demonstration PA modeling studies, and provides guidance for inclusion of the THM components in PA modeling.

This report is the final report of the BMT2 of DECOVALEX III and its counterparts in BENCHPAR, WP2, with studies performed for establishing approaches for upscaling the hydro-mechanical properties of the fractured rocks and their impacts on far-field performance of potential radioactive waste repositories.

L. Jing
F. Kautsky
J.-C. Mayor
O. Stephansson
C.-F. Tsang

January 2005

Stockholm, Sweden

Summary

The Benchmark Test 2 of DECOVALEX III and Work Package 3 of BENCHPAR concerns the upscaling THM processes in a fractured rock mass and its significance for large-scale repository performance assessment. The work is primarily concerned with the extent to which various thermo-hydro-mechanical couplings in a fractured rock mass adjacent to a repository are significant in terms of solute transport typically calculated in large-scale repository performance assessments. Since the presence of even quite small fractures may control the hydraulic, mechanical and coupled hydro-mechanical behaviour of the rock mass, a key of the work has been to explore the extent to which these can be upscaled and represented by 'equivalent' continuum properties appropriate PA calculations. From these general aims the BMT was set-up as a numerical study of a large scale reference problem. Analysing this reference problem should:

- help explore how different means of simplifying the geometrical detail of a site, with its implications on model parameters, ("upscaling") impacts model predictions of relevance to repository performance,
- explore to what extent the THM-coupling needs to be considered in relation to PA-measures,
- compare the uncertainties in upscaling (both to uncertainty on how to upscale or uncertainty that arises due to the upscaling processes) and consideration of THM couplings with the inherrent uncertainty and spatial variability of the site specific data.

Furthermore, it has been an essential component of the work that individual teams not only produce numerical results but are forced to make their own judgements and to provide the proper justification for their conclusions based on their analysis. It should also be understood that conclusions drawn will partly be specific to the problem analysed, in particular as it mainly concerns a 2D application. This means that specific conclusions may have limited applicability to real problems in 3D. Still the methodology used and developed within the BMT should be useful for analysing yet more complicated problems.

Several conclusions can be drawn from the individual team analyses as well as from the interaction discussions held during Workshops and Task Force meetings:

- Interpretation of given data constitutes a major source of uncertainty. During the course of the project it was certainly felt that these interpretation uncertainties could have a large impact on the overall modelling uncertainty.
- Differences between teams in estimated effective permeability appear to depend essentially on whether the team used given apertures as input - and then calculated fracture transmissivity using the cubic law – or if the hydraulic test data were used to calibrate the fracture transmissivity distribution. Furthermore, the assumptions used as regards fracture size versus aperture (or permeability) are not fully proven. Different assumptions on this would, although not really tested in the Task, lead to large differences in upscaled properties.
- The calculated effective rock mass deformation modulus differs between teams but all teams include the "given" value of the test case. It appears that this problem is relatively "well behaved".

- If modelling uses relaxed initial apertures as input the HM coupling is essential for capturing realistic permeabilities at depth. However, this does not necessarily imply that the HM couplings need to be considered. The fact that the aperture versus stress relation reaches a threshold value indicates that the more normal practice of fitting hydraulic properties to results of hydraulic tests is warranted! A key process, where there still is uncertainty is the relation between hydraulic residual aperture and maximum mechanical aperture, Rb. Evidently this has a strong influence on the impact of the HM coupling. Related to this is the indication found on the significance of the increase of differential stress results in increasing the permeability (when applying the non-linear stiffness model for fractures) and in channelling of flow path (potentially caused by fracture dilation).

Despite the relatively limited amount of large scale analyses conducted within the Task, some general remarks seem possible. It is suggested the stress is so high at the depth of the repository that fractures are almost completely compressed mechanically and the permeability is approaching its residual value. Therefore further stress increase due to thermal stresses would not significantly reduce the permeability. Also the TH effects, due to buoyancy, are relatively limited and would add an uncertainty in the order of a factor of 2 or so.

These observations support the conclusion that it is the uspcaling of hydraulic properties rather than the added complication of T and M couplings, which are the main sources of uncertainty in a problem of this nature. The added disturbance, in relation to in-site stress, is small in the far-field of a deep repository. Yet, understanding the stress/permeability relation is important for understanding the nature of the permeability field.

It can also be noted that most conclusions to be drawn from the large scale analyses could already be drawn from studying the intermediate performance measures such as permeability, deformation modulus and k versus stress relations.

Sammanfattning

Denna rapport sammanfattar resultaten från beräkningsfallet BMT2 inom projektet DECOVALEX III (motsvarar WP3 inom projektet BENCHPAR). Inom detta beräkningsfall analyseras i vilken utsträckning olika termo-hydro-mekaniska (THM) kopplade processer har betydelse for masstransporten i större skala från ett slutförvar i sprickigt berg.

Eftersom även små sprickor kan tänkas påverka grundvattenströmning och bergmekanik har arbetet fokuserat på hur inverkan av små sprickor kan ”skalas upp” till ekvivalenta egenskaper för bergmassan. Beräkningsfallet har därför lagts upp som en numerisk studie av ett referensproblem. Studien har haft följande mål:

- undersöka hur olika sätt att förenkla den geometriska detaljerna i bergbeskrivningen ”uppskalning” inverkar på modellprediktioner av betydelse för funktionen hos ett geologiskt djupförvar
- undersöka i vilken utsträckning, i relation tilll förvarsfunktionen, THM-kopplingar därvid behöver tas med
- jämföra osäkerheterna i uppskalningen och THM-processerna med den ofrånkomliga osäkerheten och rumsliga variationen i platsdata.

En viktig del av arbetet har dessutom varit att de olika deltagande grupperna inte bara genomför numeriska beräkningar, men tvingats göra egna bedömningar och underbygga slutsatserna från deras analyser.

Flera olika slutsatser kan dras från arbetet:

- Tolkning av data utgör en stor källa till osäkerhet.
- Skillnaden mellan olika gruppers uppskattade effektiva permeabilitet verkar bero på om man använt (uppskattade) sprickaperturer eller resultatet av faktiska hydrauliska tester som indata.
- Relationen mellan spänning och sprickapertur är osäker – och har stor betydelse för resultatet av kopplade beräkningar. En tillhörande fråga är den aperturförändring som uppstår vid skjuvdeformationer. Denna kan vara klart större en påverkan från normalspänningen och kan dessutom ge permanenta effekter.
- Om beräkningarna utgår från obelastade sprickaperturer är det synnerligen väsentligt att ta hänsyn till den hydromekaniska kopplingen för att beskriva permeabilitet och grundvattenströmning på stort djup. Men det betyder inte att denna koppling måste tas med vid all modellering. Om beräkningarna istället baseras på faktiska uppmätta hydrauliska egenskaper vid aktuella djup har denna koppling redan tagits om hand i fältdata. Då är kopplade beräkningar inte nödvändiga. För det aktuella fallet gäller speciellt att spänningarna på djupet är så höga att sprickaperturerna redan nått sitt residualvärde. Ytterligare spänningsökningar kommer därvid inte att påverka permeabiliteten nämnvärt.
- Uppskattad effektiv elasticitetsmodul för bergmassan varierar mellan grupperna, men inom ett begränsat intervall.

De gjorda observationerna ger därvid stöd till slutsatsen att det är uppskalningen av de hydrauliska egenskaperna, snarare än T och M kopplingen, som är den dominerande osäkerheten i denna typ av problem. Störningen från ett förvar är begränsad i

fjärrområdet. Det hindrar inte att relationen mellan spänning och permeabilitet är viktig för att förstå karaktären av permeabilitetsfältet.

Contents

1 Introduction

This report concerns the upscaling of thermo-hydro-mechanical (THM) processes in a fractured rock mass and its significance for large-scale repository performance assessment as studied in the BMT2 Test Case in the international DECOVALEX III project and in WP3 of the EU-funded BENCHPAR project. Different research teams have conducted the work and the details of analysis are reported separately by each team. This report focuses on the lessons learnt.

1.1 Objectives and setup of the task

BMT2 of DECOVALEX and WP3 of BENCHPAR are primarily concerned with the extent to which various thermo-hydro-mechanical couplings in a fractured rock mass adjacent to a repository are significant in terms of radionuclide solute transport typically calculated in large-scale repository performance assessments (PA). Since the presence of even quite small fractures may control the hydraulic, mechanical and coupled hydro-mechanical behaviour of the rock mass, a key aspect of the work has been to explore the extent to which these can be upscaled and represented by 'equivalent' continuum properties appropriate for PA calculations.

It must be understood that this task, even when simplified to two dimensions, is both intellectually and mathematically extremely challenging and at the limit of current computer hardware and software capability. For this reason the objectives have not been framed in absolutist terms of 'how to upscale' but rather to investigate how the uncertainties inherent in the upscaling process impact on the derived PA-relevant parameters.

Given this, the task has two, closely integrated aims:

- To understand how an explicit acknowledgement of the need for upscaling of coupled processes alters the approach to performance assessment modelling and the analysis of the model results;
- To understand the uncertainty and bias inherent in the outputs from performance assessment models in which the upscaling of THM parameters is either implicit or explicit.

From these general aims the task was set-up as a numerical study of a realistic large-scale reference problem, see Chapter 2 below. Analysing this reference problem should:

- help explore how different means of simplifying the geometrical detail of a site, with its implications on model parameters, ("upscaling") impacts model predictions of relevance to repository performance.
- explore to what extent the THM-coupling needs to be considered in relation to PA-measures.
- compare the uncertainties in upscaling (both to uncertainty on how to upscale and uncertainty that arises due to the upscaling processes) and consideration of THM couplings with the inherrent uncertainty and spatial variability of the site specific data.

Furthermore, it has been an essential component of the work that individual teams not only produce numerical results but are forced to make their own judgements and to provide the proper justification for their conclusions based on their analysis.
Finally it should be understood that conclusions drawn will partly be specific to the problem analysed, in particular as it mainly concerns a 2D application. This means that specific conclusions may have limited applicability to other problems in 3D. Still the methodology used and developed within the Task should be useful for analysing yet more complicated problems.

1.2 Participating teams

In total eight different teams analysed the Task either as part of DECOVALEX III (five teams) or as parts of BENCHPAR (three teams). ***Table 1-1*** provides the name of the teams as well as full reference to the individual team report.

Table 1-1. Teams and references to the team reports

Team	Acronym used in this report	Part of	Reference to team report
INERIS/ANDRA, France	Ineris	BENCHPAR	Progress report 1st of April 2002 Final report .1st of October 2003
Kyoto University/ JNC, Japan	JNC	DECOVALEX	Kobayashi et al. (2003)
KTH/SKI, Sweden	KTH	BENCHPAR	Last provided progress report (January 2003)
DOE/LBNL, U.S.A.	LBNL	DECOVALEX	First draft final report from DOE/LBNL, June 2002
AECL/OPG, Canada	OPG	DECOVALEX	Draft final report prepared by AECL for OPG (Chan et al. October 2003), Guvanasen and Chan (2004)
Uppsala University/STUK, Finland	STUK	DECOVALEX	Last progress report (may 2003), some data from PR 5.5.2001
Univ. of Birmingham/Nirex UK	UoB/NIREX	DECOVALEX	Progress Report 2002, Draft version 2.0 PhD thesis (October 2003) (Blum, 2003)
UPV/ENRESA, Spain	UPV	BENCHPAR	Gómez-Hernández, and Cassiraga (2004)

2 The Reference Problem

The problem addressed concerns a hypothetical heat producing repository placed at depth in a hypothetical fractured rock. However, in order to get realistically complex and spatially varying geologic data, the hydrogeologic and hydromechanical input data were loosely based on the basement geology around Sellafield, United Kingdom, and on the site characterisation data acquired by Nirex. However, it must be emphasized that the geometry analysed is purely fictional and does not represent the actual conditions at Sellafield.

A key characteristic of the rock mass considered is that the fracture density and fracture size both show fractal behaviour. This is not unusual for such rock types, but implies that there may not be a scale at which equivalent continuum behaviour exists. Further, it might be predicted a priori that spatial scales at which continuum behaviour is shown might differ for thermal, mechanical and hydrological properties, as for many individual couples.

2.1 Problem to be analysed

The reference problem concerns the far-field groundwater flow and solute transport for a situation where a heat producing repository is placed in a fractured rock medium. Radionuclides potentially released from the repository may migrate with the groundwater flow and thus reach the biosphere. Specific issues at stake are:

- how to assess the far-field hydraulic and transport properties when most data stem from small scale (borehole) tests,
- what is the impact of potential mechanical and hydraulic couplings, and
- if MH or HM couplings are significant how would they affect the upscaling?

The reference problem geometry is shown in Figure 2-1. It is assumed that the HLW (heat source) is encased within resaturated bentonite within a repository drift shown as a simple horizontal body. (NB no attempt is made to represent repository detail such as deposition holes etc.). The repository sits within a low permeability fractured rock unit which is overlain by a second low permeability fractured rock unit that extends to ground surface. A vertical fracture zone cuts both rock units but lies beyond the end of the repository tunnel.

The repository is assumed to comprise of 60 uniformly distributed canisters of HLW embedded in compacted and resaturated bentonite, with a canister density of $6 \cdot 10^{-3}$ canisters/m^2 (or 60 canisters per 100 m x 100 m). Figure 2-2 shows the heat evolution versus time for each canister.

2.2 Input Data

The relevant data for the rock formations and fault are based on Sellafield site characterisation data acquired by Nirex. The data are in the form of statistical distributions of properties. Typically, most of the data concern measurements on a small scale, whereas the problem to be studied mainly concerns the large scale.

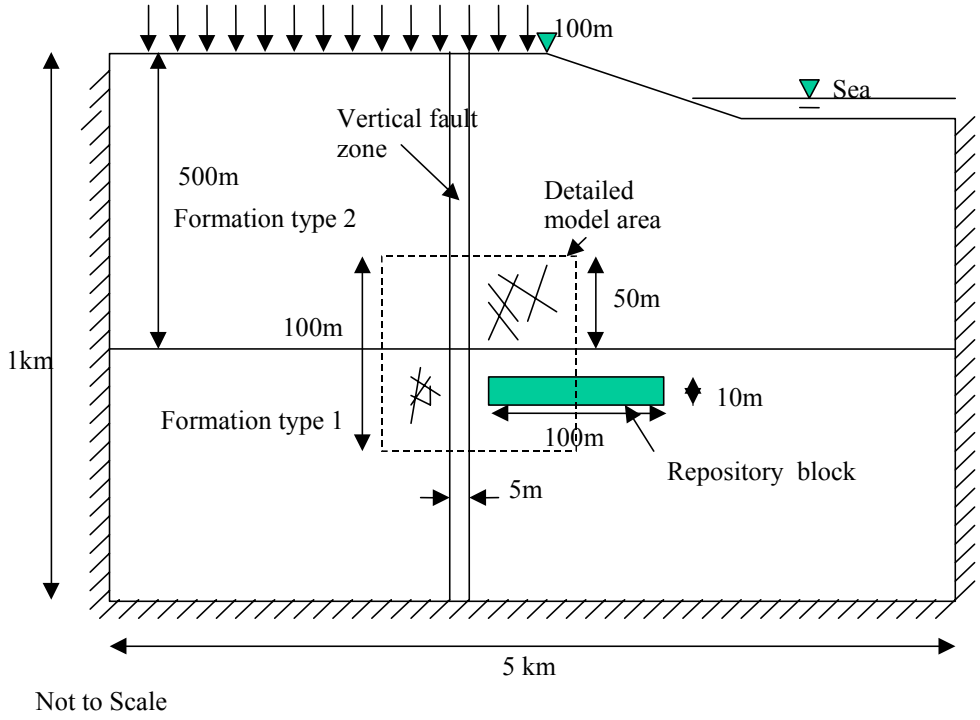

Figure 2-1: Reference problem geometry

2.2.1 Fracture statistics

2.2.1.1 Fracture orientation

The orientation data were extracted from Nirex (1997a). The orientation data and the dispersion are set-dependent and are presented for the two formations and the fault zone in

Table *2-1*, Table 2-2 and Table 2-3, respectively.

2.2.1.2 Fracture lengths

Fracture length data was obtained from analysis of 1-dimensional scan-line data at outcrop, 2-dimensional outcrop trace maps and 2-dimensional aerial photography lineaments [Nirex 1997e, page 46]. Combined data sets obtained from the above sources, for all fracture orientations, show a power law distribution of fracture (trace) lengths such that the number of fractures per km^2 of length greater than L(m) is given by:

$$N = CL^{-D} \tag{2.1}$$

where N is the number of fracture (traces) per km^2 of length L(m), C= $4\ 10^6$ and D=2.2 [+/- 0.2] [for a 2-dimensional fracture network], respectively.

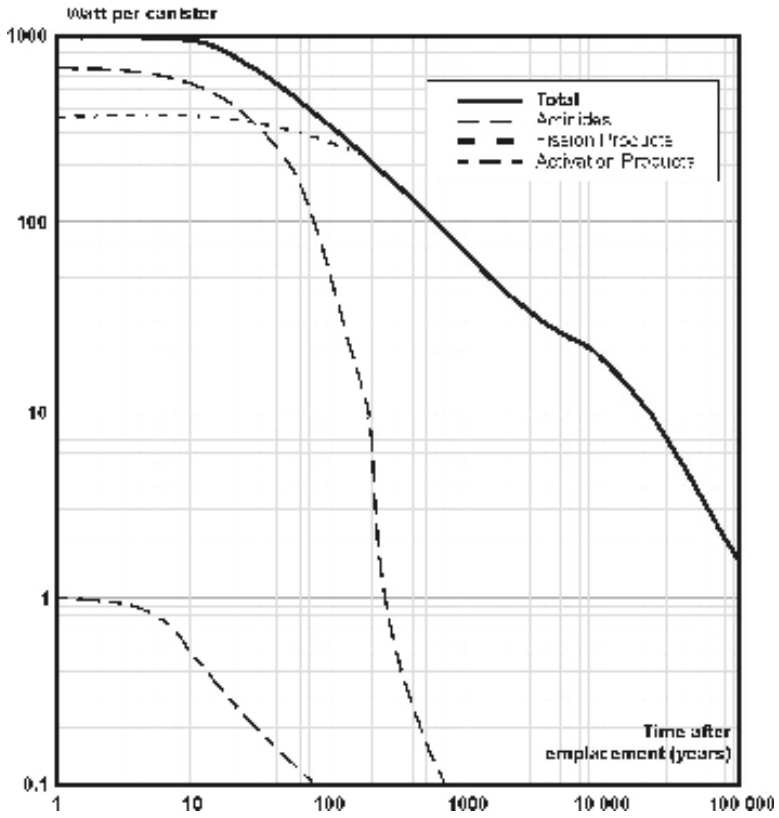

Figure 2-2: Heat source – each canister

Table 2-1. Fracture orientation for Formation 1

	Mean dip (º)	**Dip direction (º)**	**Fisher K_w**
Set 1	08	145	5.9
Set 2	88	148	9
Set 3	76	021	10
Set 4	69	087	10

Table 2-2. Fracture orientation for Formation 2

	Mean dip (º)	**Dip direction (º)**	**Fisher K_w**
Set 1	25	028	7.2
Set 2	81	156	9.4
Set 3	72	020	11
Set 4	68	090	8.1

Table 2-3. Fracture orientation for the Fault Zone

	Mean dip (º)	**Dip direction (º)**	**Fisher K_w**
Set 1	08	021	6.8
Set 2	76	150	11
Set 3	72	021	13
Set 4	74	085	6.9

These data sets did not include fractures of very small trace length. For consistency it is recommended that the above relationship should not be extrapolated to fractures with trace lengths less than 0.5 m.

2.2.1.3 Fracture frequency and fracture density

Linear fracture frequency is expressed by means of mean and maximal vertical spacing for each fracture set in each Formation (***Table 2-4***, ***Table 2-5*** and ***Table 2-6***) [Nirex, 1997a]. The spacing is obtained from measurements done in vertical and inclined boreholes and that have been corrected using a Terzaghi correction to estimate true spacings measured perpendicular to the fracture sets.

Table 2-4. Vertical spacing data for Formation 1

	Max spacing vertical (m)	**Mean spacing vertical (m)**
Set 1	5.35	0.29
Set 2	2.21	0.26
Set 3	2.01	0.28
Set 4	3.54	0.31

Table 2-5. Vertical spacing data for Formation 2

	Max spacing vertical (m)	**Mean spacing vertical (m)**
Set 1	4.29	0.51
Set 2	2.5	0.35
Set 3	3.83	0.28
Set 4	2.26	0.41

Table 2-6. Vertical spacing data for the Fault Zone

	Max spacing vertical (m)	**Mean spacing vertical (m)**
Set 1	1.43	0.18
Set 2	1.41	0.18
Set 3	1.06	0.19
Set 4	1.32	0.22

Fracture density has been shown to be a function of sampling technique, in particular the lower cut-off in the smallest fracture size included in the fracture sample is directly related to fracture density. Compilation of outcrop, borehole, aerial photography and structural maps suggests that the relationship for 2-dimensional surfaces is of the form [Nirex 1997f]:

$$density(m^{-1}) = 2.4 \cdot x^{-E} (= 2.4 / x) \qquad (2\text{-}2)$$

where x is the cut off (m) and E is a power law exponent = 1.

A 2-dimensional fracture density can be derived for any specified fracture cut-off length. The same relationship should be taken as representative of both Formations and the Fault Zone. As noted in the previous section it is recommended that a lower cut-off in fracture length used in modelling should be set at 0.5 m.

2.3 Performance measures

The study concerns the impact on calculated performance of coupled processes and associated upscaling strategies – not what is a 'strictly correct' means of upscaling. The significance of different assumptions and methods used in the upscaling should thus be compared through specified measures relevant to the performance being explored (far-field flow and solute migration). Furthermore, some intermediate measures, i.e. resulting upscaled parameter values are worthwhile to comparing.

2.3.1 Overall performance measures

Ultimately, the performance measure for a repository PA would be doses or risk, however, in order not to introduce too many assumptions about the waste, release mechanisms or the retention properties of different solute species the general performance measures studied here were restricted to the groundwater specific contribution to retention. The research teams were thus asked to predict performance measures using the following strategy.

In several different publications Cvetkociv et al. (1999) showed that the breakthrough along a single streamline essentially depends upon two different parameters:

$$\tau = \int 1/v(s)ds \tag{2-3}$$

$$\beta = \int 1/(v(s)b(s))ds = \int 1/Q_2(s)ds \tag{2-4}$$

where v(s) is the fluid velocity along the streamline, b(s) the fracture aperture and $Q_2(s)$ (m^2/s) the specific flow rate. (The total flow rate in fracture Q is given by $\int Q_2(w)dw$ integrated perpendicular to the streamlines in the fracture). Interpretation of the parameters in equations (2-3) and (2-4) are that the τ is the transit time (distribution) for a particle(s) in the flowing water and β describes the retardation capacity of the rock matrix. The parameter β is called the "transport resistance".

In practice it turns out that β is by far the most important parameter of the two since it relates to the possibilities for interaction between the flowing water and the rock matrix. In the safety assessments carried out in Sweden and Finland, it is this retention (diffusion into the matrix combined with sorption inside the matrix), which has effect on reducing releases. It can be shown that β is equal to the product $a_w t_w$ used to in the far-field migration code used in SKB SR 97 (SKB, 1999), WL/Q used in safety assessments in Finland (see e.g. Vieno and Nordman, 1999) or $a_r L/q$ used in SKI SITE-94 (SKI, 1996).

Consequently teams were asked to provide *both* "transit time (τ) distributions" and "transport resistance (β) distributions" at two output surfaces:

- a perimeter surface at 50m outwards from the boundary (wall/floor/roof) of the repository.
- the land/sea floor surface.

2.3.2 Intermediate performance measures

It turns out that most upscaling techniques lead to the formulation of effective permeability, effective rock mass deformation modulus or effective porosity to be used in large scale numerical models. Consequently, it is usually possible to directly compare two different upscaling approaches by comparing the resulting effective parameters. In fact, during the course of work, such intermediate parameters comparisons have been a more practical, and quicker tool, than the ultimate comparison of the overall performance measures.

3 Approaches to upscaling

This chapter discusses the different approaches to upscaling and subsequent problem analysis used by the different teams.

3.1 Overall approach

At a simplistic level the analysis may be considered to comprise a number of steps:

1. Analyse the rock mass fracture, hydraulic, thermal and mechanical, data provided by Nirex and abstract appropriate parameters. Derive appropriate conceptual and mathematical models.
2. Derive a description at the small scale using discrete fracture network approaches (2D or 3D) or by continuum analyses.
3. Derive upscaled equivalent hydraulic, mechanical and coupled hydro-mechanical properties for the small scale description. This involves analysis at a range of scales to ensure that appropriate representative upscaled equivalent continuum parameters are derived (the REV). This is a non-trivial exercise since there is no guarantee that there is such a scale, it may vary between properties and existing software places limits on the number of fractures that can be considered so that some form of simplification may be necessary. Clearly some uncertainty may be introduced in this step
4. Parameterise a large-scale continuum model with values obtained from step 3 and analyse the importance of the various couples in the rock mass surrounding a deep repository to determine their importance on solute transport properties at a PA scale.

These steps are further outlined in the following sections.

3.2 Small scale analyses

In general the teams have applied three different approaches to analysing the small scale data: crack tensor theory, discrete fracture network simulations and continuum approaches.

3.2.1 Crack tensor theory approach

Two teams (OPG and JNC) applied the crack tensor theory (Oda, 1986) for deriving effective permeability and rock mass mechanical properties, but the JNC team later discarded this approach.

The OPG approach was based on Oda's Crack tensor theory, extended to include thermohydromechanical parameters (Guvanasen and Chan 2004). Two types of aperture, mechanical and hydraulic, are used in the extended theory. Parameters based on the extended Crack Tensor Theory – bulk elastic properties, permeability, porosity are dependent on effective stress. The extended Crack Tensor Theory has been implemented in the FRACTUP code. An approximation of the FRACTUP upscaling

calculation has been incorporated into AECL's MOTIF finite-element code for THM modelling.

3.2.2 Discrete fracture network approaches

Several teams tried to describe the fractures statistically by a Discrete Fracture Network (DFN) model and then use the DFN-model as input to hydraulic and mechanical analyses to derive effective permeability and rock mass mechanical properties at different block sizes.

- Ineris generated DFN simulations in 3D with the RESOBLOK computer code, and determined equivalent parameters in different size models. The 3D DFN models were used as input for H- and HM computations in 3DEC. Due to software and hardware limitations, upscaling was limited to at most 5 m cube scale, and most often only at 2 m cube scale, depending on the parameter. No REV could be reached.
- JNC applied a numerical Pixel methods for the examination of the scale effect. JNC generated 3D fracture network in 60 m cube, and then extracted data for 2D fracture density, length and intensity on the model plane. A vertical 2D plane located at the centre of the model was defined and divided into 20 cm pixels. Sub-regions of different scales were randomly produced from this plane (from 5*5 to 30*30 m sizes), the size of the pixel was the same for all sub-regions. The pixel method is based on evaluation of hydraulic and mechanical processes on the 60 m plane and its sub-regions. The number of fractures existing in each pixel was counted and the permeability was assumed proportional to the number of fractures in each pixel. The model was calibrated by assigning permeability for each pixel in the different model sizes according to fracture information, and the effective permeability for the sub-regions at different scales was then calculated.
- KTH generated fracture networks in 2D and the 2D models were then used as input to UDEC for hydraulic and mechanical calculations. The determination of equivalent properties for a REV was based on stochastic realisations of the DFN at different scales (from 0.25 m to 10 m square). The DFN models were generated within 300*300 m boxes to avoid boundary effects.
- STUK split the problem into a hydrological part (H) and a thermo-mechanical part (TM). The hydrological approach was based on 3D DFN models (FracMan-Mafic) with multiple stochastic realisations to determine the directional hydraulic conductivity versus angle plots that allow examination of the validity of the continuum approximation at a 7.5 m scale. Fracture transmissivity was derived from the hydraulic borehole data. Hydraulic aperture for fractures was calculated from the transmissivity by the cubic law, under an assumption of parallel plates. Particle tracking at the same scale was also performed using hydraulic apertures. M and TM analyses were performed with a separate large model using UDEC (2D) to explore the effect of excavation, backfilling and heating on fracture apertures at various locations and for different main fracture orientations. These results were transferred to the hydrological small scale model as a sensitivity study.
- UoB/NIREX generated 2D fracture networks, with power-law fracture length distributions as input in UDEC for THM analysis. The limitations of UDEC in flow calculations and representativity of a DFN model greater than 10 m x 10 m were overcome by developing the fracture flow code FRAC2D. H analyses were

performed with constant hydraulic aperture in order to determine effective hydraulic permeability tensors. HM-analysis was performed by linking UDEC-BB with FRAC2D and then estimating the modified effective permeability tensors. Some TM- and TH-analyses would be possible with UDEC and could be conducted on modified apertures due to thermal processes.

3.2.3 Continuum approaches

Two teams applied continuum approaches:

- LBNL applied an upscaling method based on a Heterogeneous Porous medium model and Fractal Levy-stable distribution at the 1.56 m scale chosen to make use of a series of short interval hydraulic tests. Upscaling was performed by numerical experiments and stochastic simulations. The stochastic simulations are based on a fractal Levy distribution for permeability at the support scale (1.56 m) up to the grid block scale (up to 50 m). A stress-permeability relationship was added to the analysis. Particle tracking was conducted on each numerical gridblock in order to fit a gridblock scale dispersivity distribution.
- UPV applied Laplacian upscaling to 50 m blocks for average flow reproduction. Upscaled K is the ratio of total flow to head gradient.

3.3 Large scale analyses

The general approach to the large scale analysis has been rather similar between the teams, although different software has been used. It appears that differences in results (see next chapter) depend generally on differences in input parameters rather than in different codes used.

The teams have used the following approaches:

- Ineris compared T, TH, TM and THM computation using an equivalent medium code (FLAC3D). The equivalent properties derived from the upscaling.
- JNC evaluated the large scale problem with scaling rules obtained from Crack Tensor theory, but used the mean values provided in the Task.
- KTH applied the equivalent parameters from small scale analysis in THM coupled FEM code (ROCMAS) based on continuum media. At first stage non coupled hydraulic, mechanic and thermal analysis were done based on the protocol's definition and parameters.
- LBNL employed multiple realizations of subsurface heterogeneity to determine the mean flow and transport processes and the associated uncertainties. T2R3D (Wu et al., 1996) was used to simulated coupled TH and tracer transport processes - with and without heat. A sensitivity study on the influence of fracture porosity was conducted.
- OPG incorporated an approximation of the FRACTUP upscaling algorithm developed for small-scale analysis into the THM simulator MOTIF. MOTIF was applied to examine the macro-scale impact of TH(HT) HM(MH) and THM processes on the migration of radionuclides. Three sets of large-scale simulations were undertaken:

1. Nirex rock mass parameters given in the Problem Definition and Description were directly input into MOTIF for H only, TH (HT), HM (MH) and THM analyses.
2. HM (MH) and THM simulations were performed with effective rock mass permeability, porosities and deformation moduli calculated at each time step for every element in the large-scale model. All fractures were considered to contribute to the rock mass properties.
3. As in 2) above except that only 1/3 of all fractures were assumed to be active.

- STUK applied TOUGH2 to solve the head and flux field, with upscaled parameters of effective conductivity and correlation structures for the 7.5 m scale that are obtained from the DFN modelling. Transport was modelled by particle tracking, using the conductivity, head and flux fields from the hydraulic simulations and distributions of transit time and transport resistance at the 7.5 m scale from the DFN modelling. Multiple realisations, only concerning H and transport, have been conducted but TM effects were studied as sensitivity analysis based on input permeability distributions.
- UoB/NIREX: Upscaled HM-modified, effective hydraulic conductivity tensors (k_{eff}) were evaluated at REV scale (10 m × 10 m), which could be used in the regional continuum model. The continuum flow and transport code FAT3D was used for the far-field studies.
- UPV solved the full problem using a detailed description of the hydraulic conductivity field and by using an upscaled description. The results were then compared.

4 Upscaling from detailed data into effective parameters

This chapter discusses the results from the upscaling of the detailed scale data into parameters amenable for large scale numerical analysis, i.e. into effective permeability and deformation (tensors).

4.1 Fracture statistics

Many upscaling approaches were built on the fracture statistics. However, as the fracture data were given as observations and not as prescribed fracture statistical distributions, different teams made different interpretations of the data.

4.1.1 Fracture orientation

Fracture orientations were provided for each fracture set in the input data description and are presented in section 2.2.1. The way the different teams treated and applied the discontinuity orientations data is reviewed briefly below. The approaches are summarised in Table 4-1.

Table 4-1. Approaches on fracture orientation

Team	Source for orientation	Application
Ineris	Orientations as given in Task	3D generation (Resoblok)
JNC	Orientation as given in Task	3D generation
KTH	Orientation as given in Task	2D DFN model
LBNL	Not used	-
OPG	Orientation as given in Task	3D
STUK	Orientation as given in Task	3D DFN generation (FracMan)
UoB/Nirex	Orientation as given in Task	2D fracture generation (FracFrac) using a constant fracture set orientation
UPV	Not used	

INERIS: The fracture orientation was treated in 3D and the values are taken from the protocol. Fisher dispersion was taken into account.

JNC: The fracture orientation was generated in 3D according to the orientation distribution given in the Task input definition. 2D vertical planes were extracted from these 3D models for further analyses.

KTH: The KTH team generated the fractures in 3D on the basis of dip and dip direction of each fracture set as given in Table 2-1 to Table 2-3, and their Fisher coefficient. Then orientations of generated fractures were converted from 3D data into 2D using the following formula:

$$\tan\beta = \tan\alpha\cos\theta \qquad (4\text{-}1)$$

with β=Apparent dip angle, α=True dip angle, θ=Angle between the model plane (159°/90°) and the dip direction of the fracture sets. All four sets were modelled in KTH team analysis since the density of all four fracture sets were considered to be the same.

OPG: The fracture orientation was treated in 3D using data given for all four fracture sets in the Task definition. Fisher dispersion was taken into account.

STUK: For hydraulic analyses the STUK team used the Task defined orientations (Table 2-1 to Table 2-3) in 3D and generated 3D DFN models. For the 2D mechanical analysis the 3D orientations of the 3 sets were rotated in the perpendicular direction to the model plane while the dip remained unchanged.

UoB/NIREX: The UoB/Nirex team transformed the 3D orientation data given in the Task definition into 2D by projecting the 3D mean dip angles onto the 2D-model plane adopted. The conversion was done using equation (4-1).

The statistics of transformed fracture orientation were then used to generate 2D DFN models. The 4th fracture set was neglected in the 2D models because it showed almost the same strike and dip as the model plane. Two options were developed in the Fracture Network Generator to account for dispersion of fracture orientation (expressed by the Fisher coefficient in Table 2-1 to Table 2-3): i) no account was made for dispersion and only the mean apparent dip angle was used for each fracture set; ii) dispersion was considered and the Fischer coefficients were used to generate the apparent dip angles for each fracture set.

The coefficients defined in Table 2-1, Table 2-2 and Table 2-3 illustrate a fairly high dispersion of fractures in each fracture set. Nevertheless visual comparisons of DFN generated with the Fisher distribution and the trace maps clearly indicate that a high dispersion of orientation does not produce synthetic networks that are comparable to those observed. It is apparent that fracture orientation dispersion is length dependent with low dispersion of longer fractures and higher dispersion of shorter fractures.

Remarks: Essentially, the teams have used the orientation distribution as given in the test case definition. However, there is room for interpretation on how to use these distributions, which are given in 3D, for the 2D applications followed by some teams.

4.1.2 Fracture size

According to the Task input definition the fracture length distribution can be described by a Power Law function, see equation 2-1. Most of the teams used the equation with a transformation of length units, i.e.:

$$N(L) = 4L^{-2.2} \tag{4-2}$$

where N(L) is the cumulative number of fractures per m^2 of length greater than L(m). The mean fracture length, μ_L, derived from this equation is expressed as:

$$\mu_L = \frac{D}{D-1} L_{\min} \tag{4-3}$$

where L_{min} is the cut-off min applied for the fracture length distribution. The way the different teams interpreted and applied the fracture length distribution law is briefly described below and the approaches are summarized in Table 4-2.

Table 4-2. Approaches on fracture size estimation

Team	Distribution	C	D	Cut-off length min	Cut-off length max	Mean trace length	Comment
Task data	Power law	4	2.2	0.5		-	
Ineris	Power law	4	D_1=1.2 D_2=0.7 D_3=1.1 D_4=1.1	0.5	-	-	D values for each set, formation 1
JNC	Power law	4	2.2	0.5	250 m	0.92	
KTH	Power law	4	2.2	0.5	250 m	0.92	2D
OPG	Power law	4	2.2	0.5	-		
STUK, all fractures	Power law	4	3	0.5	>200	-	2D cut-off, 3D D parameter
STUK, conductive fractures	Power law	4	3	0.83	>200	-	2D cut-off, 3D D parameter
UoB/Nirex	Power law	4 3.23 1.2	2.2 2.08 2.2	0.5 0.5 0.5		0.92 0.96 0.92	Task data, 2D (Max) Mean Low
LBNL	Not used	-	-	-	-	-	-

STUK: The 3D fracture length distribution used by the STUK team is based on the 2D power law relationship that uses an exponent and a cut-off radius (equation 4-2). The 3D fractal exponent D was simply extrapolated by adding 1 to the fractal dimension of the 2D length distribution given in the Task problem definition. The fractal exponent D is given to be 2.2 [±0.2]. However, because of software limitations the Power Law exponent was stated as 3. The cut-off diameter in 3D was extrapolated from the 2D cut-off trace length by a factor 1.6. The cut-off radius was then half the cut off diameter extrapolated from the given value in the Task problem definition.

Considering all fractures (conductive and non conductive), min cut-off and max cut-off length of 0.5 and 250 m were used, which means that the equivalent 3D min radius cut-off is 0.4 m (=0.25*1.6).

From an 'OSNES analysis' the proportion of conductive fractures was estimated to be 40% of all fractures. The removed non-conductive fractures are predominantly short fractures and the adjustment of the fracture length distribution for conductive fractures was made by increasing the cut-off radius in the model. The new cut-off can be calculated from the primitive of equation 4-2 expressed as:

$$N(L) = -\frac{4}{1.2} \cdot L^{-1.2} \tag{4-4}$$

By considering the standard cut-off values, N(L) was expressed by (N(250)-N(0.5)) distribution. Taking away 60% of the non-conductive fractures towards the small fractures N(L) was expressed as 0.6*(N(250)-N(Lmin,cond)) distribution. By combining this expression to equation 4-4 the 2D length cut-off is 0.83 m. The fracture trace length distribution was then based on equation 4-2, but using a min length cut-off of 0.83 m and a max length cut-off of 250 m. The corresponding 3D min radius cut-off being used was 0.65 m, while the maximum radius was never used, since the side length of the cubic DFN realizations was only 20 m.

KTH: The 2D fracture trace length distribution used by the KTH team is based on the Power-law distribution (equation 4-2) with fractal coefficient D of 2.2 and constant C of 4 as given in the Task definition. A max and min length cut-off of 0.5m and 250m were used for the generation of the size distribution. Fracture length was generated in the model from the inverse form of the cumulative distribution function derived from equation 4-2 and the expression is:

$$L = \left(cut_{\min}^{-2.2} - F\left(cut_{\min}^{-2.2} - cut_{\max}^{-2.2} \right) \right)^{-\frac{1}{2.2}} \quad (4\text{-}5)$$

where L is the fracture length and F is a random number.

The mean trace length was calculated on the basis of equation 4-3 and is 0.92m.

INERIS: The Ineris team used the fracture size distribution defined by a Power law function (equation 4-2). A min cut off of 0.5 m is used. The coefficient C is 4 as defined in the Task. The fractal dimension D was specified for each fracture set. D for sets 2, 3 and 4 were based on information given in the Task and extracted from Nirex, 1997e. D for set 1 of all formations was estimated (no values are provided). Fracture networks with threshold length at 0.25, 0.5 and 1 m were also generated for sensitivity analyses.

UoB/NIREX: In its first evaluation the UoB/Nirex team used the Power-law function as defined in the Task (equation 4-2) with C=4, D=2.2. Based on equation 4-3, μ_L=0.92m. The Power law parameters provided are defined on a combination of data sets. However the further investigations showed that these mean data are only appropriate if the data set of the trace map is not considered. The team decided to conduct sensitivity analysis on C and D that can be inferred from the data sets, and that give low, middle and upper values for the function parameters, and as such new equations for fracture length and values for the mean fracture length:

- lower case: $n(L)=1.2 \cdot L^{-2.2}$; μ_L=0.92m
- mean case: $n(L)=3.23 \cdot L^{-2.08}$; μ_L=0.96m
- higher case: $n(L)=4 \cdot L^{-2.2}$; μ_L=0.92m

The fractures were generated in the 2D DFN models according to these Power Law equations, and two options were available: 1) cut-off min (0.5 m) and no cut-off max; 2) cut-off min (0.5 m) and cut-off max (250 m).

JNC: The JNC team used a fracture length distribution based on the power law function (equation 4-2). The length of fractures was truncated at 0.5 m and 250 m. The mean fracture length was calculated from equation 4-3 and is 0.92 m. The length of fractures was generated from the following equation:

$$L = \left\{ \left(4 \cdot (0.5)^{-2.2} - R_0^1 P_{20} \right) \frac{1}{4} \right\}^{-\frac{1}{2.2}} \quad (4\text{-}6)$$

OPG: OPG obtained a 2D surficial fracture trace length distribution using the BMT2-defined power law with exponent equal to 2.2 and a cutoff length of 0.5 m. The 2D fracture length distribution (chord of a circular disc) was translated into diameter distribution for respective circular fractures.

In summary, and as is evident from Table 4-2 the given data could lend itself to different interpretations. To some extent, but not only, this is due to whether the

subsequent analysis was made in 2D or 3D. Of particular interest are assumptions made on correlation between size and hydraulic properties as (at least implicitly) assumed by e.g. the STUK team. Clearly, the Task input data set was ambiguous with regard to this – and the resulting differences in interpretation may be seen as a reflection of this uncertainty.

4.1.3 Fracture density and intensity

There are various ways of describing fracture density or fracture intensity. A useful notation[1] was introduced by Dershowitz (1985) and later developed in the manual to the DFN-code FracMan (e.g. Dershowitz et al., 1995):

- P_{10}= number of fractures per length (number of fractures/m), ("fracture frequency"), also called P_{11} by INERIS.
- P_{20}=number of fractures per area, (number of fractures /m^2),
- P_{21}=total trace length per area, (m/m^2), also P_{22} (INERIS)
- P_{30}=number of fractures per volume (number of fractures /m^3), ("fracture density"), equivalent to P_{31} defined by INERIS.
- P_{32}=total fracture surface per volume (m^2/m^3) ("fracture intensity")

Evidently, P_{10}, P_{20} and P_{21} all depend on the direction of the observation line or plane (and of the fracture orientation distribution). Furthermore, Dershowitz (1985) shows that there is a linear relation between e.g. P_{10} and P_{21} and between P_{21} and P_{32}, whereas the relation between P_{30} ("fracture density") and P_{10} ("fracture frequency") strongly depends on the fracture size distribution.

The fracture frequency in 2D (P_{20}, number of fractures/m^2) can be calculated from equation 4-2 and taking into account the cut-off min and cut-off max. The following expression is then used:

$$P_{20} = 4\left(L_{\min}^{-2.2}, L_{\max}^{-2.2}\right) \tag{4-7}$$

with L_{min} and L_{max} respectively cut-off min and cut-off max. This expression gives an estimation of the number of fractures of all sets.

The fracture density in 2D, P_{21}, can be derived from this expression:

$$P_{21} = \mu_L P_{20} \tag{4-8}$$

with μ_L mean fracture length as defined in equation 4-3. The approach undertaken by the different teams is presented below and the summary is illustrated in Table 4-2

INERIS: The Ineris team obtained the linear fracture frequency P_{10} (P_{11} in the Ineris team notation) from vertical borehole analysis extrapolated from diagrams provided in the Task specification The min cut-off is 0.5 m. P_{10} for all fracture sets in formation 1 is 1.97 m^{-1}. The linear fracture frequency was also estimated (from the same aforementioned figure) for models generated with threshold at 0.25 and 1 m.

[1] The FracMan modelling team has unfortunately not been fully consistent in their use of this notation. In some publications they denote the total fracture length per area by P_{22}, i.e. what we here call P_{21}.

P_{21} (called P_{22} by the team) was obtained from measurements on horizontal 2D map analysis and estimated from equation 2-2 for Lmin=0.5m to: $P_{21,m}$=5 m/m^2.

The input required in the 3D fracture generator is the 3D fracture frequency, P_{30} (called P_{31} by the team). The value of P_{30} was chosen by calibration on simulation results in order to fit the measured values of P_{10} and the estimated value of P_{21}. For the first run the value of P_{30} has been set equal to P_{10} (P_{30}=2 /m^3). Then sampling on several horizontal cross-sections was done to check the correspondence of the simulated P_{30} to P_{21}. The back-calculated values from simulations of P_{21} and P_{30} were consistent with measured data of P_{21}. P_{21} was estimated from simulations to 4.39 and 5.01 m/m^2 for cubes of respectively 3 and 4m side sizes, and P_{32} to 4.74-5.39 m^2/m^3 for the same cube sizes. The fracture intensity P_{32} was determined from the RESOBLOCK simulations.

KTH: The team calculated the fracture frequency in 2D, P_{20}, on the basis of equation 4-7. The resulting P_{20} was18.38 fractures/m^2 applying L_{min}=0.5 m and L_{max}=250 m. Assuming an equal frequency of fractures in each fracture set P_{20} per fracture set is equal to 4.6 fractures/m^2. The team used the same equation (4-8) to calculate the 1D fracture frequency and the 2D fracture density. P_{21}=P_{10}= P_{20}*μ_L = 16.91 m^{-1}. The value of P_{10} can be compared to the estimated value from the vertical mean spacing (given in the protocol), P_{10}=14.1/m for formation 1.

STUK: The input parameter required by FracMan is P_{32}, which is unknown but can be calibrated against mean vertical spacing using to the following expression:

$$P_{32} = \frac{C_{p3}}{S_f} C_{p3} P_{10} \tag{4-9}$$

Using the mean vertical spacing values listed in Task protocol P_{32} was calibrated with C_{p3} of 0.843 with an r^2 value of 0.999. P_{32} is defined for each fracture set by best fit estimation from several realisations of the 3D fracture model, and by sampling: 1) perpendicular mean fracture spacing, 2) 2D fracture intensity (sampling on horizontal trace planes) and 3) mean vertical spacing. The references are P_{21}=4.8 m^{-1}, P_{10}=5.53 fractures/m and mean vertical spacing as given in the protocol. P_{21} is the mean value estimated from equation 2-2 for a min cut-off of 0.5 m. P_{10} is the vertical fracture frequency for all sets in one formation.

The fracture intensity P_{32} for conductive fractures was estimated by reducing the P_{32} for all fractures by the amount of non-conductive fractures according to the following relationship.

$$\frac{P_{10}^{cond}}{P_{10}} = \frac{2.25}{5.53} = \frac{P_{32}^{cond}}{P_{32}} = \frac{P_{21}^{cond}}{P_{21}} \tag{4-10}$$

UPV: Fracture information was used to define the ranges of the variograms used to generated the spatial distribution of heterogeneous conductivities. After several tests and the recommendation by the steering committee hydraulic conductivities were generated using a variogram with vertical anisotropy and ranges of 20 m in the vertical direction and 10 m in the horizontal.

UoB/Nirex: The fracture density in 2D, P_{21}, was estimated using two approaches. In the first approach the fracture density was derived from the Power Law distribution by applying equations 4-7 and 4-8, and using a min cut-off of 0.5 m and a max cut-off of 250 m. As mentioned in section 4.1.2 three sensitivity cases were considered that

define low, medium and high density cases. Different values of P_{20} and P_{21} were then calculated for the three different cases:

- lower case: For C=1.2 and D=2.2, P_{20}=5.51 m^{-2}, P_{21}=5.05 m^{-1}
- mean case: For C=3.23 and D=2.08, P_{20}=13.66 m^{-2}, P_{21}=13.15 m^{-1}
- higher case: For C=4 and D=2.2, P_{20}=18.38 m^{-2}, P_{21}=16.91 m^{-1}

The fracture density was estimated from equation 2-2. Applying a lower cut-off of 0.5 m, the fracture density P_{21} is 4.8 m^{-1} with a maximum of 10 m^{-1} and a minimum of around 2 m^{-1}. The three cases illustrate the sensitivity of fracture data analysis to the choice of the Power Law length distribution. The fracture density calculated for the lower case, P_{21}=5.05 m^{-1}, is close to the mean measured and given fracture density (extrapolated from a figure given in the Task definition), P_{21}=4.8 m^{-1}. The mean vertical fracture spacing was calculated for each formation and compared to the measured mean vertical spacing data provided in the Task protocol. The mean vertical spacing was estimated from vertical boreholes data adjusted according to a Terzaghi correction. The data were analysed statistically and the best-fit PDF was achieved by an exponential distribution.

The second approach used the data provided in the protocol for mean vertical spacing and transformed these by projecting the 3D fracture spacing onto the project plane using the following equation:

$$S_\alpha = S_t \frac{\cos\alpha}{\cos\beta} \tag{4-11}$$

with S_t mean true spacing (m), S_a mean apparent spacing, β apparent dip angle and α true dip angle. The apparent mean spacing was used for weighting the density of fractures in each set when using the calculated P_{20} as input for generation of fractures.

JNC: The 2D fracture frequency P_{20} was calculated using equation 4-7, applying a min cut-off of 0.5 m and a max. cut-off of 250m. P_{20}=18.4 fractures/m^2 for all sets. The 2D fracture density, P_{21}, was derived from equation 2-2. Applying this equation and using a min cut-off of 0.5 m this leads to P_{21}=4.8 m^{-1}. This value was compared to the value calculated based on the Power Law distribution of fracture length, equation 4-8. Using a min cut-off of 0.5 m and a max cut-off of 250 m the calculated P_{21} for all sets then is 16.9 m^{-1}. Since the discrepancy in P_{21} was considered as an uncertainty for fracture information both definitions are examined and their influence on upscaling results considered.

OPG: OPG determined P_{30} and P_{32} by analyzing the given surficial data to obtain the distribution of fracture diameter and density.

Table 4-3 summarizes values of fracture density estimated by different teams.

4.1.4 Spatial distribution, termination and shape of fractures

The various assumptions made on the spatial distribution of fractures can be summarised as follows:

JNC: The JNC team distributed the centre of fractures randomly in the 3D model and the fractures were assumed to be circles.

Table 4-3. Fracture density and intensity measures used

Team	P_{10} (#/m) vertical	P_{20} (#/m^2)	P_{21} (m/m^2) horizontal	P_{30} (#/m^3)	P_{32}(m^2/m^3)	Comment
Task data			5.0 (for cut-off 0.5 m)			$P_{21} \propto x^{-E}$ Mean min spacing S_f, for each set provided
Ineris	1.97 1.97 2.9 1.03	- - - -	4.4 5.01 - -	2.4 2.12 2.9 1.03	4.7 5.39 - -	3 mcube, computed, L_{min}=0.5 m 4 m cube, computed, L_{min}=0.5 m L_{min}=0.25 m L_{min}=1 m
JNC	-	18.4	4.8 16.9		-	Using equation 2-2 Using equation 4-8
KTH	16.9 14.1	18.4	16.9	Not used	Not used	Calculation based on equation. KTH only analyses 2D data. Based on mean spacing vertical.
OPG	1.96 – 5.56	0.0 – 18.38 median = 9.19	4.8 (using the recommended cutoff length of 0.5 m)	1.87-5.70 (for each set) 10.32-21.46 (for each formation)	1.1-3.4 (for each set) 6.2-12.8 (for each formation)	P_{20} range given for various fracture lengths. Range for other measures represents variation among formations and sets.
STUK	5.53 2.25	- -	*4.8* -	- -	11.9 4.46	All fract, lower formation, parameters used as input for DFN modelling Cond. fract, lower formation, parameters used as input for DFN modelling
UoB /Nirex	not used	5.5 13.66 18.38	5.05 13.15 16.91	Not used	Not used	lower case (to fit measured P_{21}), C=1.2, D=2.2 mean case, C=3.23, D=2.08 Higher case, C=4, D=2.2
LBNL	-	-	-	-	-	Not used
UPV	-	-	-	-	-	Not used

STUK: The STUK team assumed circular disk fractures. The STUK team also considered the data on fracture termination. The data on fracture terminations were used for the spatial generation of the 3D DFN model. 27% of the fractures were generated from uniformly located fracture centres, while the remaining 73% were generated from locations uniformly distributed on surfaces on existing fractures.

KTH: For the KTH team no spatial distribution was assigned for the generation of fractures in space so fractures are randomly distributed in the model.

INERIS: The Ineris team considered the fractures as polygons. Fracture density P30 (P31 in INERIS notation) is assumed to follow a Poisson law;

UoB/NIREX: The UoB/Nirex team generated fractures following a Poisson distribution. A development of the algorithm for generating midpoints of fractures by the repulsion method has been completed (Chillingworth, 2002). However, the repulsion algorithm was not used in the task.

OPG: The OPG team represented fractures by circular disks. Only disks with centroids located within the averaging volume were used.

Remarks: The spatial model chosen for the generation of fractures might have a significant influence on the calculation and simulation of effective hydraulic conductivity. Again, there are differences between teams, which originate from assumptions (necessary) rather than from hard data.

4.2 Hydraulic upscaling

The approach to hydraulic upscaling differs between teams using DFN-analyses and the teams using a porous medium approach only. The latter only considers the hydraulic measurements in the different scales, whereas the former combines the model of the fracture network with the hydraulic information for the upscaling.

4.2.1 DFN and Crack Tensor Theory approaches

Various approaches to upscaling into effective permeability based on DFN-modelling or other discrete techniques have been applied by the teams. These are outlined below:

JNC: JNC used a pixel method for upscaling hydraulic properties and conducted a sensitivity study on the influence of fracturing. The pixel method, applied in 2D, was based on 3D DFN realisations generated according to fracture information in 150 m cubes. The reference plane for the pixel method was chosen as the centre vertical section. This original plane was divided by pixels of 0.2 m square. The hydraulic conductivity of each pixel is proportional to the number of fractures counted in this pixel and related to the average measured logarithm of permeability and its standard deviation. The scale effect was studied in sub-regions from 5 m*5 m up 60 m *60 m size, representing the finite element mesh on the original plane divided into pixels of equal dimension. The vertical and horizontal 1D flow was examined in each sub-region by applying a hydraulic gradient equivalent to the length of the sub-region. The equivalent permeability of a sub-region was obtained as an average velocity at the outlet boundary based on unit hydraulic gradient and identical element size. The scale effect was studied by the variation of the average and standard deviation of homogenized permeability for different size sub-region. The average homogenized permeability slightly increases with scale while the standard deviation decreases much with scale. The permeability calculated for each sub-region could be identified as the effective parameter if its value coincides with the geometric mean. Tests conducted on the 5 and 30 m sub-regions showed that this approximation might be true.

Sensitivity to upscaling was tested by dividing the large region (60 m x 60 m) in sub-regions and trying to estimate the effective permeability of the large region consisting of sub-regions. Each sub-region has an effective permeability value given from the pixel method described above. The same hydraulic boundary conditions were set to the sides

of the large region model. The results show that the geometric mean has a good agreement with the effective hydraulic conductivity especially for sizes greater than 5m. Since the geometric mean coincides with the effective hydraulic conductivity the lognormal distribution can be appropriate for the hydraulic conductivity distribution in sub-regions.

KTH: The KTH team analysis was based on multiple stochastic realisations of 2D DFN model. For each realisation in a 300*300 m^2 square, scale models ranging from 0.25 to 10 m are extracted and for each model the directional permeability was calculated by applying specific pressure boundary conditions in UDEC. Constant hydraulic aperture for zero normal stress was calculated as arithmetic mean of the data from the four tested cores, and set to 65 μm. The investigations on the applicability of continuum approach was also studied by rotating each DFN model stepwise 30° and comparing the result with the one predicted by second order permeability tensor transformation. The evaluation of directional permeability was based on the extended Darcy's law for anisotropic homogeneous media. The simulations showed that the directional permeability decreases as the model size increases but becomes constant beyond a certain size, which indicates the existence of a REV. The presence of the equivalent permeability tensor (and so the existence of a REV) was demonstrated if the calculated directional permeability values and the average permeability tensor conform to an ellipse. Based on results of previous simulations an equivalent permeability tensor was reached when the model size was equal to or greater than 5m, and a REV can be given with acceptable variation and prediction error.

INERIS: The hydraulic analyses of the Ineris team are based on DFN models and 3DEC simulations. 3 different boundary conditions are applied in 3DEC to determine the equivalent permeability tensor. The analyses were based on 5 stochastic realisations of DFN models at each model size (from 2 to 5 m). For each model size, the equivalent vectorial flow rate was averaged from the flow rate value at different locations of the fracture network after each computation at different boundary conditions. A constant hydraulic aperture was assumed. However, computer limitations made most of the realisations at 3 and 4 m scale impossible to evaluate. The permeability tensors calculated at three model sizes (2, 3 and 4 m) showed that the values change with size but remain in the same order of magnitude. Running more models at bigger scale than 2 m are required to be able to determine the REV and check whether the components of the permeability tensor come to an asymptotic level. Also the impact of artificial joint prolongations and fracture length threshold was investigated. The prolongation of joint up to the next block face (that artificially increased the fracture network connectivity) could lead to overestimate the permeability by a factor of 2 or 3. Increasing the fracture threshold length seems to increase the permeability, whereas the number of fractures in the model decreases. The problem might be related to independent simulations of fracture network for the different tests, and the minimum fracture length approaching the size of the model.

OPG: The OPG team developed a permeability field by applying Guvanasen and Chan's (2004) modification of Oda's crack tensor theory. The test scale was a 100 m x 100 m model. Input data include the rock matrix elastic constants and fracture set geometric and mechanical data. Mean data provided in the Task are used for the rock matrix mechanical properties. Distributions of fracture geometry properties given in the Task definition are used whenever available. The Cumulative Distribution Function for hydraulic aperture was estimated from the BMT2-given transmissivity distribution (inferred by Nirex from short-interval hydraulic pulse tests). The interpretation of the tests was made assuming that all fractures within a single test interval have the same

hydraulic aperture. The in situ stresses under which the pulse tests were conducted were determined using the BMT2-defined relationships between depth and stress components. Hydraulic and mechanical apertures under various effective stresses were calculated using the Barton-Bandis empirical constitutive relationships.

STUK: The STUK team conducted the hydraulic upscaling in a sequence of steps:

1. The fracture T-distribution was fitted so as to reproduce borehole hydraulic measurements based on a probabilistic approach (Osnes analysis in the FracMan software). The frequency of conductive fractures, n, and a lognormal distribution for the fracture transmissivity distribution (defined by mean value and standard deviation) were found by iteratively searching for the best fit between packer test and a distribution of Monte Carlo simulated T values. The best fits obtained for a vertical frequency of conductive fractures was used as input for the DFN models and the 3D small scale analyses. The hydraulic analyses were conducted in 3D to estimate the directional conductivity of the fracture network when changing the model plunges from 0 to 165° in a vertical cross section parallel to the large scale modelling plane. The simulated network was 7.5*7.5*7.5 m^3, extracted from 20 m cube generated DFN realisations. The directional conductivity was calculated according to Darcy's law. Very low transmissivity fractures were removed from the models in order to make the computer simulations more tractable. The simulated conductivity was then compared to the 2D symmetric conductivity tensor for continuum media. The conclusions of these analyses were that directional conductivities at this scale can be approximated by symmetrical conductivity tensors, and the obtained effective conductivities were jointed into one probability distribution for input to large scale simulations.
2. Particle tracking simulations were conducted at a small scale to estimate distributions of transit time, τ, and transport resistance, β. The tests were performed in a 7.5*7.5*7.5 m^3 volume, with guard zones in the transverse direction of flow. 30 fracture networks are extracted from 30 realisations of the DFN model in 40m cubes. Each model was rotated in a vertical cross section parallel to the large scale modelling plane. A large number (10 000) of particles were released through a 2*2 m^2 window and particles collected at the remaining sides of the transport region were counted. The simulations showed that the distribution of transit time and transport resistance can be expressed as single probability distribution $G(\tau K_{eff}^{2/3})$ and $G(\beta K_{eff})$.
3. The small scale procedure was repeated on 10 of the previous fracture networks to study the influence of TM effects on directional conductivities. These fracture networks were selected to be representative for all the previous networks, regarding anisotropy and continuum appearance. No TM effects were applied to set 4 in these fracture networks, since it was neglected in the 2D TM modelling. The analysis showed that the effective conductivity is decreased by almost 40-50% close to the repository but minor changes are measured at distance.

UoB/NIREX: The hydraulic analyses used by the UoB/Nirex team for the determination of the REV was based on multiple simulations with FRAC2D. To evaluate the 2D permeability tensor for square domains the boundary conditions were adjusted to give head gradient directions between 0° and 150° in 30° steps. The Darcian flow law was assumed to calculate the conductivity tensor coefficients (k_{xx}, k_{xy} and k_{yy}). The DFN model was generated in a 100 m × 100 m box, and all sizes were extracted from this network. The simulations showed that permeability decreased as model size increased, which was related to disconnection of the boundaries through long fractures.

The REV was considered to be achieved if the cumulative variances of the principal permeability tensors and of the principal directions were each time less than 5% of the cumulative averages. A REV could not be achieved for the low-density cases below a block size of 100 m × 100 m, but could be achieved for medium and high density cases at model sizes greater than 10 m (except Formation 2, mean density where the REV was achieved for the 15 m × 15 m model). Analyses with DFN generated at constant fracture set orientations and generated accounting for Fisher dispersion show that the REV was achieved at the same conditions. An alternative upscaling method must be developed for the low density case. For all density cases the initial hydraulic aperture will be changed based on results from HM analyses.

4.2.2 Continuum approaches

Two teams tried continuum approaches for the hydraulic analysis, i.e. they worked directly with the small scale permeability data collected from the field and did not use the geometry data from the different sets of fractures.

LBNL: The LBNL team fitted a Levy-stable Fractal distribution to small-scale permeability short interval tests (length interval 1.56 m) performed in one vertical borehole. These data were collected from the lower formation, but the fractal parameters defined from the distribution were assumed to be valid for all formations. Nevertheless the mean permeability was specific for each formation. The simulations for upscaling were based only on small-scale conductivity data and do not consider fracture geometry. The model was built by computationally generating the spatial variability of permeability in gridblock size corresponding to the measurement interval (1.56 m) in the whole model domain. The effective permeability was calculated in gridblocks ranging from 1.56 to 50 m, while the heteoregeneous distribution of permeability was always generated in 1.56·1.56 m gridblocks. A simple numerical approach was used to estimate the effective hydraulic conductivity. No flow conditions were applied on the top and bottom boundaries while a gradient head was applied on the sides. The conductivity was calculated according to Darcy's law. In order to determine the dispersivity the gridblocks were conceptualised as "homogeneous" effective porous medium and particles were introduced at the inflow boundary of the model. Transport time to the outflow boundary wss recorded and the longitudinal dispersivity was calculated from the breakthrough curve.

UPV: Multiple realizations of conductivity distributions with a vertical anisotropy of 20 m to 10 m and with varying means and variances were generated over a discretization of the domain in cells of 5 m by 5 m. In each realization groundwater flow and flow resistance were computed. Then, a Laplacian approach was used to upscale the conductivities at the 5 m by 5 m scale into blocks of 50 m by 50 m (a scale suitable for PA analysis in the sense that the final number of discretization blocks is small). Grounwdater flow and flow resistance were computed on the upscaled fields and it was found that there is a need to include a fictitious retardation factor in order to match the flow resistance curves. This retardation factor depends on the underlying variance of the hydraulic conductivities at the small scale, going from 1 for a homogeneous field up to 1.6 for a variance of 1.

4.2.3 Resulting effective properties

Table 4-4 shows calculated effective permeability in one of the formations (Formation 1) for the different approaches. There are some clear differences between the teams. The following can be noted:

- It is judged that differences between teams essentially depend on whether the team used given apertures as input - and then calculated fracture transmissivity using the cubic law – or if the hydraulic test data were used to calibrate the fracture transmissivity distribution. Still, also for teams using the hydraulic information, the deviation between teams is at least an order of magnitude – and significantly lower than the effective permeability given in the test case definition!
- The teams have not really validated assumptions as regards fracture size versus aperture (or permeability). Different assumptions on this would, although not really tested in the Task, lead to large differences in upscaled properties. While calibrating against single hole hydraulic tests would take away most uncertainty as regards the stress/aperture impact, this is not the case as regards the size/aperture relation!

Table 4-4. Formation 1 permeabilities at different scales

Team	mean k (m^2)	$m_{log\ k}$	s_{logk}	Scale	Notes
Task data	$5.7\ 10^{-18}$	-17.25	0.48	50 m?	*Based on Nirex, 1997*
INERIS	$k_{xx}=1.4\ 10^{-13}$	-12.85	-	2 m	*…artificial joint prolongation*
	$k_{xx}=5.5\ 10^{-14}$	-13.26		2 m	*…without joint prolongation*
	$k_{xx}=1.6\ 10^{-13}$	-12.8	-	3 m	*…with joint prolongation*
	$k_{xx}=1.3\ 10^{-13}$	-12.9	-	4 m	*…wiith joint prolongation*
JNC	$6.25\ 10^{-18}$	-17.21	0.22		*Mean value constant at different scales, but s dependent on the scale. Input 030331*
KTH	$k_{xx}=3.5\ 10^{-16}$ $k_{yy}=3.4\ 10^{-15}$	-15.5 -15.5	< 0.05	5 m	*2D, DFN, constant aperture but by considering stress effect on finite fractures*
LBNL		-18.98	C_0=0.47	1.56	*1.56 m scale, C_0 fractal parameter*
		-18.9	1.14	50·12.5	*50 - 12.5 m scale (Based on numeric simulations)*
OPG	$4.7\ 10^{-17}$ to $7.2\ 10^{-17}$ ($7.4\ 10^{-18}$ to $1.2\ 10^{-17}$)	-16.2 (-17.0)	n.a.	10 – 100 m	*At 500m depth. Values in parentheses assuming 1/3 of fractures unfilled and conductive. Range covers diagonal elements of permeability tensor. Convergence analysis (0.5 to 1000 m) indicated convergence when the upscaling length ~3 m.*
STUK	$8.610*10^{-19}$	-18.1	0.32	7.5 m	*3D DFN 7 m block*
		-18.0	0.08	50 m	*Further upscaling by stochastic continuum from 7.5 m scale.*
		-19.2	0.03	50 m	*Packer data (non correlated)*
		-19.2	0.16	50 m	*Packer data (18 m correlated)*
UB	$k_{xx} = 3.510^{-16}$ $k_{xy} = 5.010^{-17}$ $k_{yy} = 5.510^{-16}$	-15.5 -16.3 -15.3	-	10 m	*Permeability Tensors for Formation 1 in 750 m depth, medium-density case, 10 m domain size (REV)*
UPV		-17.25	0 - 1.0	5. m 50 m	*October 2001, Sensitivity study*

4.3 Mechanics upscaling

4.3.1 Discrete approaches

Several teams used DFN-modelling or other discrete techniques for upscaling into effective rock mass deformation properties:

KTH: The method used by the KTH team is based on multiple stochastic realisations of 2D 300*300 m DFN models[2]. For each DFN realisation different model sizes (from 0.25 to 10 m) were extracted. The compliance matrix was resolved by applying 3 linearly independent boundary conditions to the discretised DFN model (BC1: biaxial stresses, BC2: sequentially increased vertical stress, BC3: sequentially superimposed shear stress over stress conditions from BC2). Input data for intact rock and fractures were taken from the test case core samples. The investigation of applicability of a continuum approach was also studied by rotating the model stepwise through 10° and comparing the results with the one predicted by fourth order compliance tensor transformation. The effects of the ratio normal stiffness/shear stiffness on the elastic properties of the rock mass were also studied. Elastic modulus (in x and y-direction) as well as Poisson's ratio were calculated for the different DFN sizes. For a model size equal to or greater than 5 m the elastic compliance matrix can be approximated by a fourth order elastic compliance tensor. Quantitative evaluation of REV size was conducted by coefficient of variation and prediction error.

JNC: The JNC team used both pixel method and crack tensor theory for upscaling rock mass mechanics properties[2].

The basis of the pixel method is the same as described in section 4.2.1. The equivalent elastic parameter of pixels crossed by fracture(s) is calculated and the equivalent Young's modulus and Poisson's ratio of sub-regions (5*5, 25*25 and 50*50 m) can be attributed to produce the heterogeneous isotropic elastic medium. If no fracture crosses the pixel it will be assigned the properties of the intact rock. The plain strain loading tests were conducted for each sub-region and the equivalent directional Young's modulus for different model sizes was obtained. The results showed that the anisotropy of the model is very limited and that the equivalent parameter does not decrease significantly for models larger than 25 m.

In upscaling by the crack tensor theory the scale effect of fractures on JRC and JCS were accounted for on the basis of relationships between lab-scale and the Probability Density Function of fracture length. The variety of fracture length gives the scale effect of stiffness of fracture and crack tensor components. The method was based on a 3D generation of the fracture network with fracture orientation of each set was constant at a first stage, and the maximum length of generated fractures was set to the length of the model. The compliance tensor components showed a huge variation with model size. This might be decreased by taking into account the mean length of fracture for each model size and not the real length distribution. A stable value for Young's modulus and Poisson's ratio was obtained, but for model sizes that are greater than by the pixel method. The results showed that the elastic properties are isotropic.

[2]The tests as described here were conducted on DFN models generated in 250 m cubes, and the fracture length was based on an equation derived from equation 4-2. The methodology is unchanged but the results and potential conclusions might be changed in the new calculations based on fracture length generation from equation 4-2 and DFN models in 60 m cubes.

After comparison of results from both upscaling methods the input data for large scale analyses are taken from crack tensor theory results.

OPG: The OPG team determination of effective parameters was based on application of the crack tensor equations and calculations were realised with the Fractup Code. The methodology was similar to that described for hydraulic upscaling (section 4.2.1). The compliance tensor is, however, a 4^{th} order tensor whereas the permeability tensor is a 2^{nd}-order tensor. See Guvanasen and Chan (2004) for details.

STUK: No upscaling of mechanical properties

UoB/NIREX: No upscaling of mechanical properties. However, it would be possible to evaluate E and ν by using the non-linear empirical Barton-Bandis model.

INERIS: The Ineris team mechanical analyses were based on DFN simulations (model sizes from 2 to 5m) and 3DEC. Five DFN simulations have been run for each model size to assess the standard deviation of the properties. The tests have been performed by applying 6 sets of mechanical boundary conditions (no hydraulic fluid pressure) to determine the equivalent stiffness tensor. The analyses were based on 5 stochastic realisations of DFN models at each model size (from 2 to 5 m). The impact of artificial joint prolongations and fracture length threshold has been investigated on 2 m model size. The stiffness tensor was between 5 to 10% higher without artificial joint prolongations. The fracture length threshold did not appear to have a significant impact on the equivalent stiffness tensor. Considering the evolution of the terms of the equivalent stiffness tensor with the model size the REV could be guessed to be close to 5 m.

4.3.2 Continuum Approaches

LBNL: no upscaling of mechanical data

UPV: no upscaling of mechanical data

4.3.3 Resulting effective properties

Table 4-5 summarises the calculated effective rock mass deformation modulus in Formation 1, as calculated by the different teams. The predicted variability differs between teams but all teams include the "given" value of the test case.

4.4 Hydro-mechanical analyses

4.4.1 Discrete approaches

JNC: The JNC team studied the effect of stresses on fracture aperture by using the formula for aperture, JNC and JCS derived from the crack tensor theory. The results show that the standard deviation obtained on this study is very small in comparison to the measured standard variation of hydraulic conductivity. Moreover the aperture change with depth as calculated with the Barton-Bandis model is not very significant. Hence the change of aperture will be considered through the statistical distribution on aperture given in the protocol.

Table 4-5. Comparison between calculated rock mass deformation modulus (GPa) in Formation 1. Task refer to equivalent values provided in the Task definition of mechanical properties.

Team	Rock mass deformation modulus (GPa)	Notes
Task	65	Based on Nirex, 1997
Ineris	T_{xxxx} = 67 to 55 T_{yyyy} = 73 to 58 T_{zzzz} = 61 to 44 T_{xxyy} = 54 to 46 T_{xxzz} = 50 to 38 T_{yyzz} = 52 to 39	Stiffness tensors (diagonal terms of the Tijkl tensor) at 2 m to 5 m scale for formation 1 (with artificial joint prolongations and with a fracture length threshold of 0.5 m)
JNC	10 – 250	Decrease with scale! Results from PR feb.2002
KTH	E_x=34-39 (mean 36) E_y=40-44 (mean 42)	5 m scale
LBNL	-	No upscaling of rock mechanical parameters
OPG	13-17 (32-39)	Anisotropic, range over E1, E2, E3; values are given at 500 m below OD. They are depth dependent. Values in parentheses obtained assuming 1/3 of fractures are active.
STUK	-	No upscaling of rock mechanical parameters
UoB/NIREX	-	Will not be performed, but possible (time!)
UPV		Not used

INERIS: The Ineris team performed hydro-mechanical analyses (no mechanical deformation at boundaries) by applying a fluid pressure build-up in the model to determine the equivalent Biot's tensor. As the computation time turned out to be very high, simulations have only been realised on 2m scale. The mesh size seemed to have a restricted influence on the Biot's tensor. Four stochastic DFN realisations have been computed and the average Biot tensor for the model size has been calculated.
Some hydro-mechanical simulations have also been done to determine the equivalent permeability tensor considering a stress-dependent relation for hydraulic aperture. For HM computation, 3DEC consider a relation between the hydraulic aperture "a" and the mechanical aperture "u" that can be written: $a = a_0 + \Delta u$, where a_0 is the zero stress aperture. A maximum and residual aperture is considered for numerical stability reason (INERIS assumes: $a_{max} = a_0 = 6.5\ 10^{-5}$ m ; $a_{res} = 1.8\ 10^{-5}$ m). No relation was assumed between joint stiffness and stress or fracture length. Five stochastic DFN realisations were computed and the results analysed. The permeability decreases when the stresses increase but no REV could be determined. It can be notice that there is a residual equivalent permeability (around 10^{-9} m/s) that has to be related to the residual hydraulic aperture. That residual permeability is reached for $\sigma > 20$ MPa for a joint normal stiffness of $Kn = 4.43\ 10^{11}$ Pa/m.

UoB/NIREX: The HM-modelling was performed with the UDEC-BB model with aperture distributions output to FRAC2D for the hydraulic calculations. Only medium-density DFN with a block size of 10 m × 10 m were analysed. The HM modelling was carried out in a similar manner to the H modelling. Sensitivity studies were carried out to examine the impact of the mechanical boundary conditions, mechanical properties, initial mechanical apertures, aperture changes with increasing depth (HM coupling) and

various DFN with changing fracture lengths and block sizes. The two main conclusions of the HM-modelling are as follows. First, the variation of hydraulic properties as a function of depth can be identified using this modelling method with given mechanical properties and fracture geometries. Significant differences between the constant aperture H modelling and variable aperture HM modelling results are observed that lead to different large scale flow conditions. Second, the sensitivity studies revealed that the underlying variation in the mechanical properties have a significant impact on the HM-modelling. Understanding the spatial variation of the mechanical properties of the rock mass and fractures is vital to understand the connectivity of high and low permeability zones and to model the heterogeneity of the host rock at the large scale.

KTH: The KTH team performed HM analyses to capture the significance of the stress-permeability relationship. Permeability changes are estimated by applying stress boundary conditions on the DFN model. Two different stress boundary conditions are considered. First the ratio of vertical to horizontal stresses was assumed constant and was then sequentially increased. This enabled calculation of the overall change of permeability. The second method was to increase horizontal stress while maintaining the vertical stress constant. This enabled investigation of the effect of differential stress on permeability change due to dilation of fractures. Both constant normal stiffness and non-linear stiffness models were used for the behaviour of fractures. Residual, initial and maximum hydraulic apertures were given in the protocol. The simulations show that the permeability is reduced by 2 orders of magnitude when increasing the stress ratio, and the anisotropy is almost insignificant when stress ratio is close to unity. The permeability does not change beyond a stress ratio equivalent to 1000 m depth considering the effective stress. The increase of differential stress results in increasing the permeability (when applying the non-linear stiffness model for fractures) and in channelling of flow paths. The main controlling parameter is dilation of fractures when the stress ratio is high enough to cause the plastic deformation of the fractures.

OPG: The AECL/OPG team's modified crack tensor theory is a coupled THM theory. The hydro-mechanical coupling, formulated based on the Barton-Bandis empirical constitutive relationships, is inherent in the modified crack tensor equations (Guvanasen and Chan 2004). All effective rock mass properties, including permeability, porosities and mechanical compliance are dependent on effective stress and, therefore on both mechanical stress and pore pressure. Effective properties have been calculated for all 3 formations at depths ranging from 0 to 750m (corresponding to increasing effective stress). Results indicate that deformation modulus to increases with depth while both permeability and porosity decrease with depth. The stress dependency is very strong between 0 and 250 m depth (5 orders of magnitude increase in E and 4 orders of magnitude decrease in k) but very little change between 500m and 750m depth (generally within a factor of 2). This nonlinearity arises from the very nonlinear stress-fracture closure relationship.

4.4.2 Continuum approaches

LBNL: The LBNL team studied the impact of stress on permeability by performing stochastic simulations at different scales. A relationship between stress and aperture was established from available lab-scale data and was translated to a stress-permeability relationship for the 1.56 m block size. The analyses were performed as described in section 4.2.2 but the stress-permeability was added to the analysis at the 1.56 m block level and derived for the final grid blocks through the stochastic analysis. The initial

permeability field was generated from the Fractal-Levy function in the 1.56 m blocks. Then a stress change was induced and a new flow simulation was conducted to derive a new effective permeability.

Two different upscaling models were used to consider the assignment of local permeability. The most influential parameter is the ratio between hydraulic residual aperture and maximum mechanical aperture, R_b. The first model was based on the assumption that all fractures are similar and possess the same ratio R_b. In this case the permeability ratio is not scale-dependent and no upscaling is required. The second model was based on the assumption of single vertical and horizontal fractures in the 1.56 m blocks. The permeability ratio is then scale-dependent and steered by local permeability and aperture of fractures.

UPV: The UPV team decided from the onset not to upscale any mechanical data based on previous experience about the minimal impact that hydro-mechanical coupling would have in PA at the large scale

4.4.3 Remarks

Despite the preliminary nature of the HM analysis conducted, some general remarks could be made:

- If modelling uses relaxed initial apertures as input the HM coupling is essential for capturing realistic permeabilities at depth. It appears that the 2 order of magnitude decrease as e.g. noted by the KTH team would account for most of the discrepancy between their modelled (assuming relaxed apertures) and measured as seen in ***Table 4-4***. However, this does not necessarily imply that the HM couplings need to be considered. The fact that the T/stress relation reaches a threshold value indicates that the more normal practice of fitting hydraulic properties to results of hydraulic tests is warranted! Nevertheless, this raises the issue as to the extent to which hydraulic data obtained at one depth can be used in a model at a different depth if not corrected for HM-responses.
- A key process, where there still is uncertainty is the relation between hydraulic residual aperture and maximum mechanical aperture, R_b. Evidently this has a strong influence on the impact of the HM coupling. Related to this is the indication found on the significance of the increase of differential stress results in increasing the permeability and in channelling of flow path (potentially caused by fracture dilation).
- Most of the research teams applied mean mechanical properties for their HM analysis. However, the variability of mechanical properties and the impact on the performance measurements and the uncertainties were not thoroughly addressed. Some results (UB/Nirex) suggest that the impact of the variations of the mechanical properties is higher than the HM coupling.
- At the outset it was considered that the data on fracture geometry was sufficient for the task. However, it turned out that the fractal dimensions of the fracture lengths and fracture density were poorly constrained and that markedly different fracture densities could be generated that were consistent with the data.
- Few teams recognized that only a subset of fractures were actually flowing under in-situ conditions and none tried to explain why this was so. All teams treated all fractures as formed by the same genetic failure mechanism and did not distinguish joints from veins from faults. None considered different scaling laws for each type

of fracture. While it cannot be certain that such considerations would improve the predictive capability of flow and migration in fractured media, this nevertheless illustrates that modelling cannot simply be a matter of computer simulations. The actual physics of the problem and existing data ought to be considered.

5 Large scale analysis

In the large scale analyses all teams used their upscaled properties in various Equivalent Porous medium codes. Thereby they could explore the resulting effect on the large scale flow – and also explore the impact of the heat source which is part of the large scale problem.

5.1 Impact of the heat source on T, H and M properties

Most teams have studied the impact of the heat source in the large scale problem as given in the Task definition protocol.

5.1.1 The JNC team

The JNC team modelled the large scale problem according to the Task protocol, using the THM coupled code THAMES. Hydraulic conductivity was assigned to the elements of the model through the following process:

- Firstly the mean and standard deviation of permeability were identified as a function of scale, based on the upscaling analyses by the pixel method. The mean permeability slightly increases with size while the standard deviation of logarithm of permeability decreases drastically with size.
- Then the mean hydraulic conductivity was calculated for each element of the mesh according to the mesh size with the above function. By using the standard deviation of logarithm of permeability coinciding with the element size, the hydraulic conductivity for each element was generated around the above mean hydraulic conductivity with lognormal distribution.
- Since the size effect on mean permeability is small with size and the standard deviation becomes small with size, the large element mostly had the same hydraulic conductivity. On the other hand, the hydraulic conductivity of small element had a large variation even for the same size of element.

The coupled TH analyses showed that the temperature reaches its maximum at the repository after 70 years. Then the temperature increase spreads out across the entire model region. The velocity direction is first upward because of the buoyancy effect due to heat generation from the repository. The direction turns to downward after 1000 years when the hydraulic gradient becomes larger than the buoyancy effect.

5.1.2 The INERIS team

INERIS have used the fully coupled FLAC3D continuum code for the large-scale problem. The H, T, HM, TH, TM and THM aspects of the problem were considered. FLAC3D limitation are the following: permeability and porosity are not temperature or strain dependent; there is no convection; no temperature change due to M variations; the

influence of capillary pressure is neglected; the pore pressure is assumed to be zero in the unsaturated zone.

Upscaled values have been used, even if, as noted above, it was not possible to demonstrate that these were truly equivalent properties since an REV had not been demonstrated for H, M or HM properties. The fractured rock-mass is assumed to be an orthotropic, elastic porous media. The initial permeability is assumed to be stress-dependent following a relation established previously (this has been taken into account considering for each term a relation with depth).

At the state of equilibrium before the heat is activated, the intensity of these flow vectors are higher in fault zone where the permeability are 1 order of magnitude bigger than elsewhere. The intensity of the flow decrease very quickly with depth. The flow orientations also change with depth especially under the sea.

The maximum temperature (about 55 °C) is reached after 20 years at the repository centre.

If we look at the discharge vectors around the repository for THM computation, it can be noticed that, between 10 years & 100 years, the fluid is forced to go outward from the repository surrounding (due to thermal expansion) and that flow intensity decreases with time (as well as temperature gradient). At 1000 years, the flow is coming back. The TH computation didn't show any significant effect of the repository on the fluid discharge vectors.

The analysis of stress, displacement & pore pressure variation with time show that:

- hydraulics can be neglected to estimate the stress or displacement variation. Indeed, comparison between TM and THM computations shows that displacement & stress differences remain below 20 %;
- mechanics cannot be neglected to evaluate the discharge vectors and the pore pressure variation. Indeed, comparison between TH and THM computations shows completely different results.

5.1.3 The KTH team

The large scale hydraulic analyses performed by the KTH team apply boundary conditions as given in the protocol. In the current analysis the hydraulic, mechanical and thermal processes were investigated independently in the Finite Element code ROCMAS. In a planned subsequent analysis all processes will be combined in a coupled THM analysis. The mesh size ranges from 5 m close to the repository to 100 m. It is found that the temperature increases very rapidly in a limited volume close to the repository. The temperature increase reaches farther away from the repository as time increases while the highest temperature at the repository decays.

5.1.4 The LBNL team

The LBNL team used the numerical code T2R3D to simulate coupled TH analyses and tracer transport processes. Simulations were conducted using permeability values obtained by the upscaling technique developed and by applying the stress-permeability relationship established at 50-m scale (section 4.4.2). The effect of this relationship on 50-meter permeability was simulated and plotted versus depth/effective stress.

The simulations show that the stress is so high at the depth of the repository that fractures are almost completely compressed mechanically and the permeability is approaching its residual value. Therefore further stress increase due to thermal stresses would not significantly reduce the permeability.

Large-scale TM simulations were then conducted using this stress-dependent permeability relationship and conceptualising the repository as a heat source. Most changes in the permeability field occur after 1000 years when the heat transfer occurs in a larger area around the repository. Due to higher thermal stresses in the horizontal direction most changes in permeability occur in the vertical direction. The simulations suggest that the TM processes induce relatively small changes in permeability. A small reduction of permeability occurs above the repository while the vertical permeability at the ground surface is increased

The heat source problem was set up as given in the protocol. The discretisation of the model was very fine near the repository. After steady-state TH processes were achieved under ambient conditions a heat source was introduced at the repository. Since the upscaling simulations show that significant heterogeneity still exists at 50×50 m blockscale, Monte Carlo simulations were used for evaluating flow and transport processes. Multiple realisations of subsurface heterogeneity (based on mean and standard deviation for permeability at 50×50 m scale) were used to determine the mean flow and transport processes. Effects of heat released from the repository were evaluated for each realisation. The temperature increase reaches its maximum (50°C) at the repository in about 100 years. The temperature increase is first localised and then spreads out to a larger distance around the repository.

5.1.5 The OPG team

The OPG/AECL team used the Finite Element Code MOTIF. The model and the boundary conditions applied to the model were chosen according to the problem definition given in the protocol. Three sets of large-scale simulations were undertaken (Chan et al. 2003):

1. Without redoing the upscaling Nirex rock mass parameters given in the Problem Definition and Description were directly input into MOTIF for H only, TH (HT), HM (MH) and THM analyses.
2. HM (MH) and THM simulations were performed with upscaling, with effective rock mass permeability, porosities and deformation moduli calculated at each time step for every element in the large-scale model. All fractures were considered to contribute to the rock mass properties.
3. As in 2) above except that only 1/3 of all fractures were assumed to be active.

For the TH analysis without upscaling the equivalent fresh water head starts to deviate from the natural steady-state geothermal condition by a fraction of a metre about 10 years of heating and returns gradually to this steady-state geothermal condition in about 100 000 years. The average horizontal groundwater velocity in the case of TH processes is about twice the velocity for the isothermal steady-state flow, and the vertical velocity is about 40% to 70%. The temperature in the vicinity of the repository reaches a peak in about 54 years and the maximum calculated temperature is 50°C in the middle of the top of the repository block. After that the temperature increase spreads

over a larger volume of rock and after 10 000 years much of the repository heat has been dissipated.

5.1.6 The STUK team

The STUK team used the simulation code TOUGH2 for large scale continuum TH analyses. The input was the probability distribution defined from the DFN 7.5 m scale analysis and further upscaling from 7.5 m to 45 m by stochastic continuum analysis.

- In order to assign effective permeability to the elements of the model correlation structures for the effective permeability scale were studied by the indicator value method. This was done on borehole data for 1.56 m packer tests. A detailed study of the variograms showed that the spatial distribution was controlled by three populations, background permeability ($K<10^{-18}$ m/s), flowing features and indicator values. Theoretical models could then be fitted to the variograms.
- A 50 m x 50 m simulation net was generated by assembling separate stochastic realisations of indicator values, background permeability and flowing features. Flow simulations were carried out on the 7.8*7.8 m elements and the directional effective permeabilities were derived from Darcy's law. Permeability values in each element were then replaced by its effective permeability value (1 grid for each direction). Finally, variograms for these effective permeabilities were obtained and used as input for the large scale hydraulic model.

The mechanical analyses were conducted with the 2D code UDEC in order to estimate the fracture displacements in relation to the excavation and filling with swelling material.

- A large-scale model (1100*700 m) reduced from the original large scale model size (5*1 km) was built and analysed. The blocks were discretised on the basis of simplified fracture networks. Set 4 was neglected for all formations as it is almost parallel to the model plane. The 3 other sets were generated in 2D by rotating their orientations in the perpendicular direction to the model plane, the dip remained unchanged. The fracture frequency in the model was scaled on the basis of mean fracture spacing (given in section 2.2.1) in order to decrease the number of joints in the models, and the normal and shear stiffness are decreased using the same ratio. Intact rock properties were selected from wire line data provided in the protocol. A hydraulic aperture/normal stress relationship was constructed on the basis of provided test results.
- The mechanical calculations were run by simulating the excavation of the repository, the thermal modelling was executed separately on a larger distinct element model by assuming a constant heating power of the waste for 3 years and a decaying heating power for longer simulation times.
- The first results of these thermo-mechanical analyses show that the excavation and the 2 MPa swelling pressure of backfilling material have a minor effect on the stress state around the repository area. The temperature evolution is fast close to the repository (increase and then decrease) and fairly slow and constantly increasing at locations further away. Long-term heating affects hydraulic aperture and a decay of about 10-15% of apparent aperture is measured during the first 00 years of heating, which implies a decay of fracture transmissivity.

5.1.7 The UoB/Nirex team

The UoB/Nirex team used the continuum flow and transport code FAT3D for the far-field studies and particle tracking was undertaken to examine the flow paths and travel times through the repository host rock under different physical conditions. No heat source was considered due to lack of available time. The magnitude of the effective porosity was determined from a calculation of the mean advective velocity through the discrete fracture network (DFN). The same averaging scale of 10 m × 10 m was adopted for both the effective porosity and the effective hydraulic conductivity.
Two models were considered until now: (1) a homogeneous hydraulic base case assuming constant hydraulic apertures throughout the model domain and (2) a non-homogeneous hydro-mechanical base case with hydraulic apertures determined from analysis of HM coupling using the mean mechanical properties for each formation. The methodology and the results are reported in Blum et al. (2004).

5.2 Particle tracking – the overall performance measures

A few teams also conducted particle tracking in order to be able to calculate the overall performance measures as defined in section 2.3.

5.2.1 Individual team approaches

JNC: The JNC team made simulations based on results from H and T analysis, performed by simulating the liberation of 1 particle at the repository for a single pattern. The effective porosity was decided from wire line data. 20 realisations were generated based on simulations of permeability distribution. Coupled analysis and particle tracking analyses were carried out for each realisation. The total number of particles was 300. The particle trajectory was studied for different starting time (t=0, t=1000 years and t=10000 years). The trajectory is very complicated close to the repository at starting time t=0 because of the buoyancy effect. Particles go mainly through formation 2, which has a higher permeability. The transit time for travelling from the repository to the surface increases with the starting time of particles from the repository.

LBNL: The LBNL team conducted tracer transport simulations coupled to TH processes with or without heat release. The simulations show that the heat release does not have a significant effect neither on near-field radionuclide transport nor on far-field transport, and can subsequently be neglected. All simulations were based on the permeability distribution established on short-interval field measurements and a porosity of 5.7%. A sensitivity study was conducted in order to determine the impact of fracture porosity on the breakthrough curves. A model of infinite fractures in vertical and horizontal directions was assumed. The porosity was calculated based on fracture frequency and hydraulic aperture. The porosity values obtained for formations 1 and 2 were 1.6410^{-5} and 2.810^{-4}. Breakthrough curves were much shorter when using lower fracture porosity. Nevertheless thermal loading has a noticeable but insignificant effect on radionuclide transport.

OPG: The OPG team made a limited particle tracking analysis for eight different runs, inclding no upscaling, upscaling with all the fractures and upscaling assuming 1/3 of all fractures are active. Approximate upscaling is performed within the large-scale model for each element individually at every time step so as to capture the variation of effective rock mass properties with stress and pore pressure. Six particles were released from points evenly distributed over the mid-level of the repository block. They were tracked to the 50m boundary and to their discharge points at the right final boundary of the model and in the sea. THM impacts on transit time are more important at the 50m scale than at the km scale. Among the 8 simulations minimum transit time to the 50m boundary is $1/70^{th}$ of the maximum transit time. For transit to final boundary of the large-scale model the corresponding ratio is <40. The fracture density assumed in the modelling, and whether upscaling is performed or not, appear to affect the transit time to final discharge more than THM coupling. The path lengths at the different measuring points are very similar but the travel times range from about 500000 to over 900000 years.

STUK: The STUK teams performed particle tracking on the large scale model. The model was discretised into cubic blocks of 7.5 m size to be consistent to the upscaled properties. The effective permeability distribution $G(K_{eff})$, obtained from the small scale DFN simulations, was used to assign properties to the elements. A particle is released at a nodal point of a random element within the repository area and the particle is moved to the adjacent node in a given direction following a probability based on the fraction of the total outward directed flux in that same direction. Transit time and transport resistance were sampled from the probability distributions obtained from the small scale analysis. TM effects on large scale particle transport were studied using the trend in effective conductivity change established by TM-modified small scale simulations. This yielded an upper estimate of the transit time and transport resistance. The impacts are small in comparison to the intrinsic uncertainties in modelling hydraulic flow in fractured rock.

UoB/Nirex: The UoB/Nirex team calculated particle travel times (t_{50}) for the two considered base cases (H and HM base cases). For the H base case with a constant hydraulic aperture of 10 μm and a medium-density fracture network, the particle travel time from the repository to the sea bed only takes 120 years. In case of the HM base case, the particle travel time is 4,860 years, but please note that for Formation 2, the uniaxial compressive strength (UCS) of 120.0 MPa was chosen instead of 39.6 MPa due to numerical problems. Preliminary results with a UCS = 39.6 MPa showed that the particle travel time is around 372 500 years. Hence the results for the HM base case a very sensitive to the chosen mechanical properties, thus it was decided to analyse a third HM case, in which the entire range of mechanical properties is assessed in a layered stochastic continuum approach. Unfortunately, the final results cannot be reported yet.

UPV: The main objective of the UPV team was to compare the flow and transport behaviour of the study area at a small scale (5 m by 5 m discretization) and at a larger scale after upscaling (50 m by 50 m discretization) so that it can be checked whether the upscaling procedure yields comparable results at both scales. For this purpose groundwater flow and flow resistance (by particle tracking) were solved at both scales. Hydraulic upscaling was carried out using the most precise and numerically demanding techniques capable to preserve average head gradients and average flows through the upscaled blocks. Yet, it was found that flow resistance curves in the upscaled fields do not match the same curves in the small scale fields. A possible correction to obtain a fit is to include a retardation factor at the block scale as a function of the hydraulic

conductivity variance at the small scale. For this particular case, this retardation factor varies from 1 for a homogenous field up to 1.6 for a field with a variance of 1 in logK. The UPV team also conducted its analysis on multiple realizations in order to assess the degree of uncertainty about the performance measures. While these uncertainty can be computed by Monte Carlo analysis, it was found that the upscaled Monte Carlo realizations displayed less uncertainty (as measured by the spread of the flow resistance curves from the multiple realizations) than the Monte Carlo realizations at the small scale. In order for the upscaled realizations to match the uncertainty of the small scale realizations there was a need to multiply the upscaled spread by a factor similar to the retardation factor need to match the flow resistance curves.

5.2.2 Discussion

Table 5-1 summarises the breakthrough times calculated by the various teams. Differences between teams are large, but most likely due to various assumptions on porosity and on the effective permeability. The impact on the temperature field is generally not very pronounced as the teams note that:

- The simulations show that the heat release does not have a significant effect on the far-field transport, and can subsequently be neglected there.
- The fracture density assumed in the modelling, and whether upscaling is performed or not, appear to affect the transit time to final discharge more than THM coupling. Furthermore, the impact on the transport resistance is less than on the travel time.
- Hydraulic properties of fractured media are inherently dependent on stress and pore pressure through fracture aperture. Generally, it is not clear how upscaling can be done properly from small-scale fracture properties without including THM coupling in the upscaling procedure. However, the stress dependence is much less important once the stress levels are so high that fractures apertures approach their residual value, i.e. at stress levels common at potential repository depths.
- An alternative may be to infer large-scale hydraulic properties by calibration against large-scale field tests. The high induced hydraulic gradients necessary for large-scale hydraulic tests to be performed in tight rock in a reasonable time frame begs the question of whether properties calibrated to these experiments are still valid under natural conditions.

Also the UoB/Nirex team report remarkably large impacts on HM effects and the used uni-axial compressive strength. However, the H analysis, assuming hydraulic apertures of 10 μm results in orders of magnitude higher permeability at depth than recorded from the hydraulic tests. It could thus be discussed whether the comparison really is fair, see similar discussion in relation to the hydraulic upscaling, section 4.2.3.

Table 5-1. Resulting overall performance measures as calculated by the different teams

Team	τ_{50} at 50 m (in years)	τ_{50} final in years/m	β_{50} final in years/m	Comment
Ineris				Not provided
KTH				Not provided
JNC	$9.8 \cdot 10^5$ (3.110^{13} s)	$8.8 \cdot 10^6$ (2.810^{14})	$4.1 \cdot 10^{15}$	
LBNL	$(3.9\text{-}6.8) \cdot 10^4$	$(1.48\text{-}2.09) \cdot 10^4$	$(7.09\text{-}9.5) \cdot 10^8$	Only H (years)
	$6.61 \cdot 0^6$			TH
OPG	$4.85 \cdot 10^4$	$7.85 \cdot 10^5$	$2.60 \cdot 10^7$	H only, no upscaling, rock mass properties in Task[3]
	$5.95 \cdot 10^4$	$7.77 \cdot 10^5$	$2.61 \cdot 10^7$	HM, no upscaling, rock mass properties in Task;
	$3.64 \cdot 10^4$	$5.85 \cdot 10^5$	$1.94 \cdot 10^7$	TH, no upscaling, rock mass properties in Task;
	$4.34 \cdot 10^4$	$5.79 \cdot 10^5$	$1.94 \cdot 10^7$	THM, no upscaling, rock mass properties in Task;
	$8.36 \cdot 10^2$	$2.53 \cdot 10^4$	$6.75 \cdot 10^5$	HM, upscaling using all fractures;
	$7.70 \cdot 10^2$	$2.00 \cdot 10^4$	$4.70 \cdot 10^5$	THM, upscaling using all fractures;
	$4.81 \cdot 10^3$	$1.77 \cdot 10^5$	$4.69 \cdot 10^6$	HM, upscaling assuming 1/3 of all fracture active;
	$5.37 \cdot 10^3$	$1.40 \cdot 10^5$	$3.82 \cdot 10^6$	THM, upscaling assuming 1/3 of all fracture active;
STUK	500 ($1.5 \cdot 10^{10}$ s)	$1.1 \cdot 10^3$ ($3.3 \cdot 10^{11}$s)	$2.7 \cdot 10^{10}$ $7.54 \cdot 10^{17}$s	Without TM
	566 ($1.7 \cdot 10^{10}$s)	$1.2 \cdot 10^3$ ($3.58 \cdot 10^{11}$s)	$2.8 \cdot 10^{10}$ $8.12 \cdot 10^{17}$s	With TM
UoB/NIREX	-	120 yrs ($3.8 \cdot 10^9$ s)	-	H base case (constant hydraulic aperture = 10 μm).
		$3.72 \cdot 10^5$		HM with (UCS = 39.6 MPa)
UPV		$1.5 \cdot 10^8$		Only H, σ=1detailed
		$1.7 \cdot 10^8$		Only H, σ=1upscaled

5.3 Discussion

Despite the relatively limited amount of large scale analyses conducted within the Task, some general remarks seem possible:

- It is suggested the stress is so high at the depth of the repository that fractures are almost completely compressed mechanically and the permeability is approaching its residual value. Therefore further stress increase due to thermal stresses would not significantly reduce the permeability. However, one must bear in mind that thermal stress does not always increase compressive stress. In some areas there can be reduction of compressive stress. Also, in the near field where temperatures are relatively high, THM coupling through the storage term may not be negligible.
- Also the TH effects, due to buoyancy, are relatively limited and would add an uncertainty in the order of a factor of 2 or so.

[3] ; β_{50} taken as travel time with Darcy velocity

These observations support the conclusion that it is the uspcaling of hydraulic properties rather than the added complication of T and M couplings, which are the main sources of uncertainty in a problem of this nature. The added disturbance, in relation to in-situ stress, is small in the far-field of a deep repository. Yet, understanding the stress/permeability relation is important for understanding the nature of the permeability field.

It can also be noted in hindsight that some of the conclusions to be drawn from the large scale analyses could already be drawn from studying the intermediate performance measures such as permeability, porosity, deformation modulus and k versus stress relations.

6 Conclusions

Several conclusions can be drawn from the individual team analyses as well as from the interaction discussions held during Workshops and Task Force meetings.

6.1 Interpretation of Discrete Fracture Network Data

Several observations can be made as regards interpretation of Discrete Fracture Network Data. During the course of the project it was certainly felt that these interpretation uncertainties could have a large impact on the overall modelling uncertainty. More specifically,

- There has been relatively little difficulty in interpreting the orientation distribution as given in the test case definition. However, there is room for interpretation on how to use these distributions, which are given in 3D, for the 2D applications followed by some teams.
- There is considerably more uncertainty in the interpretation of fracture size. Of particular interest are assumptions made on correlation between size and hydraulic properties. Such assumptions may have a large impact on the upscaling rule.
- There was also various approaches to selecting the fracture density. Provided consistency checks are made on various measured properties, this may in fact turn out to be useful for bounding the fracture intensity used in subsequent simulations, but attention to the problem is needed since fracture intensity has a key impact resulting upscaled hydraulic and mechanical properties.
- The spatial model chosen for the generation of fractures might have a significant influence on the calculation and simulation of effective hydraulic conductivity. Again, there are differences between teams, which originate from assumptions (necessary) rather than from hard information data.

6.2 Effective permeability

The different teams' results on effective permeability show clear differences between the teams. The following can be noted:

- It is judged that differences between teams depend essentially on whether the team used given apertures as input - and then calculated fracture transmissivity using the cubic law – or if the hydraulic test data were used to calibrate the fracture transmissivity distribution. Still, for teams using the hydraulic information, the deviation between teams is at least an order of magnitude – and significantly lower than the effective permeability given in the test case definition!
- The teams have not really validated assumptions as regards fracture size versus aperture (or permeability). Different assumptions on this would, although not really tested in the Task, lead to large differences in upscaled properties. While calibrating against single hole hydraulic tests would take away most uncertainty as regards the stress/aperture impact, this is not the case as regards the size/aperture relation.

The latter observation also directly links to the question whether upscaling needs to be done using a DFN approach (which most teams applied) or if stochastic continuum approaches would suffice. It can be expected, that more extreme assumptions of the fracture size versus aperture relation would show a more dramatic difference between these approaches.

6.3 Upscaling the mechanics

The calculated effective rock mass deformation modulus differs between teams but all teams include the "given" value of the test case. It appears that this problem is relatively "well behaved".

Despite the preliminary nature of the HM analysis conducted, some general remarks could be made.

- If modelling uses relaxed initial apertures as input the HM coupling is essential for capturing realistic permeabilities at depth. However, this does not necessarily imply that the HM couplings need to be considered. The fact that the aperture versus stress relation reaches a threshold value indicates that the more normal practice of fitting hydraulic properties to results of hydraulic tests is warranted!
- A key process, where there still is uncertainty is the relation between hydraulic residual aperture and maximum mechanical aperture, Rb. Evidently this has a strong influence on the impact of the HM coupling. Related to this is the indication found on the significance of the increase of differential stress results in increasing the permeability (when applying the non-linear stiffness model for fractures) and in channelling of flow path (potentially caused by fracture dilation).

6.4 Need for coupled analyses in the far-field?

Despite the relatively limited amount of large scale analyses conducted within the Task, some general remarks seem possible:

- It is suggested the stress is so high at the depth of the repository that fractures are almost completely compressed mechanically and the permeability is approaching its residual value. Therefore further stress increase due to thermal stresses would not significantly reduce the permeability.
- Also the TH effects, due to buoyancy, are relatively limited and would add an uncertainty in the order of a factor of 2 or so.

These observations support the conclusion that it is the uspcaling of hydraulic properties rather than the added complication of T and M couplings, which are the main sources of uncertainty in a problem of this nature. The added disturbance, in relation to in-site stress, is small in the far-field of a deep repository. Yet, understanding the stress/permeability relation is important for understanding the nature of the permeability field.

It can also be noted that most conclusions to be drawn from the large scale analyses could already be drawn from studying the intermediate performance measures such as permeability, deformation modulus and k versus stress relations.

References

Blum, P., Mackay, R. & Riley, M. S. *Understanding the impact of hydro-mechanical coupling on performance assessment of deep waste disposal*. In: O. Stephansson, J. A. Hudson and L. Jing (eds.), Coupled thermo-hydro-mechanical-chemical processes in geo-systems, fundamentals, modelling, experiments and applications, Elsevier Geo-engineering book series Elsevier Ltd., Oxford, UK; 2004, Vol. 1 p.237-242. 2004.

Blum, P. *Upscaling coupled HM processes in fractured rock*. PhD-Thesis, University of Birmingham. (in progress). 2003.

Chan, T., Guvanasen, V. and F.W. Stanchell. *Final research team report on DECOVALEX III BMT2 – upscaling*. Prepared by Atomic Energy of Canada Limited and Hydrogeologic Consulting for Ontario Power Generation. Draft October 2003, Toronto. 2003.

Chillingworth, G. E. H. *The Effects of Fracture Geometry on the Permeability of Fractured Rock*. MSc-Thesis, Department of Earth Sciences, University of Birmingham, United Kingdom. 2002.

Cvetkovic, V., Selroos, J. O. & Cheng, H. *Transport of reactive tracers in rock fractures*. Journal of Fluid Mechanics, Vol. 378, pp. 335-356. 1999.

Dershowitz, W.G. *Rock Joint Systems.* PhD Thesis, Massachusetts Institute of Technology. 1985.

Dershowitz W, Lee G, Geier J, Foxford T, LaPoint P, Thomas A. *FRACMAN Interactive Discrete Feature Data Analysis, Geometric Modelling and Exploration Simulation. User Documentation, version 2.5*. Golder Associates Inc. 1995.

Gómez-Hernández, J. Jaime and Eduardo F. Cassiraga. *Impact of flow and transport coupling in the upscaling of transport parameters for performance assessment in the context of nuclear waste disposal.* . In: O. Stephansson, J. A. Hudson and L. Jing (eds.), Coupled thermo-hydro-mechanical-chemical processes in geo-systems, fundamentals, modelling, experiments and applications, Elsevier Geo-engineering book series Elsevier Ltd., Oxford, UK; 2004, Vol.1, p.243-250. 2004.

Guvanasen, V. and Chan, T. *Upscaling the thermohydromechanical properties of a fractured rock mass usig a modified crack tensor theory*. In: O. Stephansson, J. A. Hudson and L. Jing (eds.), Coupled thermo-hydro-mechanical-chemical processes in geo-systems, fundamentals, modelling, experiments and applications, Elsevier Geo-engineering book series Elsevier Ltd., Oxford, UK; 2004, Vol.1, p.251-256.

Kobayashi A., Y. Sugita and M. Chizimatsu. *Up-Scaling and Its Impact on TH Process on Performance Assessment*. Kyoto university, Japan Nuclear Cycle Development Institute (JNC), HAZAMA Corporation, JAPAN. 2003.

Nirex. *Data summary sheets in support of gross geotechnical predictions*. Nirex Report SA/97/052. 1997a-f.

Oda, M. *An equivalent continuum model for coupled stress and fluid flow analysis in jointed rock masses*. Water Resources Research, V.22, No. 13:1845-1856. 1986.

SKB. *SR 97 – Post-closure safety. Deep repository for spent nuclear fuel. Main Report (Volumes I and II).* Svensk Kärnbränslehantering AB, Stockholm. 1999.

Vieno T och Nordman H. *Safety assessment of spent fuel disposal in Hästholmen, Kivetty, Olkiluoto and Romuvaara* TILA-99, Posiva Oy, Helsinki, Finland. 1999.

Wu, Y. S., C.F., Ahlers, P., Fraser, A., Simmons, K., Pruess. *Software qualification of selected TOUGH2 modules*. LBNL-39490, Lawrence Berkeley National Laboratory, Berkeley, CA. 1996.

www.ski.se

STATENS KÄRNKRAFTINSPEKTION
Swedish Nuclear Power Inspectorate

POST/POSTAL ADDRESS SE-106 58 Stockholm
BESÖK/OFFICE Klarabergsviadukten 90
TELEFON/TELEPHONE +46 (0)8 698 84 00
TELEFAX +46 (0)8 661 90 86
E-POST/E-MAIL ski@ski.se
WEBBPLATS/WEB SITE www.ski.se